Is water vapor a key player of the wintertime haze in North China Plain?

Jiarui Wu[1,4,7], Naifang Bei[2], Bo Hu[3], Suixin Liu[1,4], Meng Zhou[5], Qiyuan Wang[1,4], Xia Li[1,4,7], Lang Liu[1,4,7], Tian Feng[1], Zirui Liu[3], Yichen Wang[1], Junji Cao[1,4], Xuexi Tie[1,4], Jun Wang[5], Luisa T. Molina[6], and Guohui Li[1,4*]

[1]Key Lab of Aerosol Chemistry and Physics, SKLLQG, Institute of Earth Environment, Chinese Academy of Sciences, Xi'an, Shaanxi, China
[2]School of Human Settlements and Civil Engineering, Xi'an Jiaotong University, Xi'an, Shaanxi, China
[3]State Key Laboratory of Atmospheric Boundary Layer Physics and Atmospheric Chemistry, Institute of Atmospheric Physics, Chinese Academy of Sciences, Beijing, 100029, China
[4]CAS Center for Excellence in Quaternary Science and Global Change, Xi'an, China
[5]Department of Chemical and Biochemical Engineering & Interdisciplinary Graduate Program in Geo-Informatics, University of Iowa, Iowa City, Iowa, USA
[6]Molina Center for Energy and the Environment, La Jolla, California, USA
[7]University of Chinese Academy of Science, Beijing, China
[*]Correspondence to: Guohui Li (ligh@ieecas.cn)

Abstract. Water vapor has been proposed to amplify the severe haze pollution in China by enhancing the aerosol-radiation feedback (ARF). Observations have revealed that the near-surface $PM_{2.5}$ concentrations ([$PM_{2.5}$]) generally exhibits an increasing trend with relative humidity (RH) in North China Plain (NCP) during 2015 wintertime, indicating that the aerosol liquid water (ALW) caused by hygroscopic growth could play an important role in the $PM_{2.5}$ formation and accumulation. Simulations during a persistent and heavy haze pollution episode from 05 December 2015 to 04 January 2016 in NCP were conducted using the WRF-Chem model to comprehensively quantify contributions of the ALW effect to near-surface [$PM_{2.5}$]. The WRF-Chem model generally performs reasonably well in simulating the temporal variations of RH against measurements in NCP. The factor separation approach (FSA) was used to evaluate the contribution of the ALW effect on the ARF, photochemistry, and heterogeneous reactions to [$PM_{2.5}$]. The ALW not only augments particle sizes to enhance aerosol backward scattering, but also increases the effective radius to favor aerosol forward scattering. The contribution of the ALW effect on the ARF and photochemistry to near-surface [$PM_{2.5}$] is not significant, generally within 1.0 μg m^{-3} on average in NCP during the episode. Serving as an excellent substrate for heterogeneous reactions, the ALW substantially enhances the secondary aerosol (SA) formation, with an average contribution of 71%, 10%, 26%, and 48% to near-surface sulfate, nitrate, ammonium, and secondary organic aerosol concentrations. Nevertheless, the SA enhancement due to the ALW decreases the aerosol optical depth and increases the effective radius to weaken the ARF, reducing near-surface primary aerosols. The contribution of the ALW total effect to near-surface [$PM_{2.5}$] is 17.5% on average, which is overwhelmingly dominated by enhanced SA. Model sensitivities also show that when the RH is less than 80%, the ALW progressively

increases near-surface [$PM_{2.5}$], but commences to decrease when the RH exceeding 80% due to the high occurrence frequencies of precipitation.

1 Introduction

Atmospheric aerosols or fine particle matters ($PM_{2.5}$) influence the climate directly by scattering and absorbing the solar radiation, and indirectly by serving as cloud condensation nuclei and ice nuclei (Ackerman, 1977; Ackerman and Baker, 1977; Jacobson, 1998, 2002; Penner et al., 2001). Moreover, high levels of $PM_{2.5}$ in the atmosphere also cause severe haze pollution, impairing visibility and exerting deleterious effect on ecological system and human health (Chan and Yao, 2008; Zhang et al., 2013; Kurokawa et al., 2013; Weinhold, 2008; Parrish and Zhu, 2009). In addition to anthropogenic emissions, the poor air quality is generally influenced by stagnant meteorological situations with weak winds and high relative humidity (RH) (Flocas et al., 2009; Quan et al., 2013; Zhang et al., 2014; Bei et al., 2016; Wu et al., 2017; Ding et al., 2017). RH, as an important meteorological factor in the atmosphere, considerably affects the formation, chemical composition, and physical properties of atmospheric aerosols (Seinfeld et al., 2001; Hallquist et al., 2009; Poulain, 2010; Nguyen et al., 2011).

As the main constituent in the atmosphere, water vapor directly participates in the atmospheric physical and chemical processes. Since many components of atmospheric aerosols are hygroscopic, they take up water as RH increases (Covert et al., 1972; Pilinis et al., 1989), thereby influencing the aerosol size distribution, chemical composition, mass concentration, and corresponding optical properties as well as radiative effects (Im et al., 2001; Carrico et al., 2003; Randles et al. 2004; Cheng et al., 2008). Wang et al. (2016) have indicated that the ratio of SO_4^{2-} to SO_2 exhibits an exponential increase with RH. Tie et al. (2017) have shown that the sulfate, nitrate, and ammonium concentrations increase from 16 to 25 μg m^{-3}, 15 to 23 μg m^{-3}, and 11 to 17 μg m^{-3}, respectively, when RH increases from 60% to 80%. Field measurements in Beijing have demonstrated that the inorganic aerosol fraction increases with increasing RH (Wu et al., 2018). In addition, water vapor also serves as an

important medium in the formation of secondary aerosols (SA) through liquid-phase reactions and heterogeneous reactions (Seinfeld and Pandis, 1986; Pilinis et al., 1989). For example, Li et al. (2017) have indicated that the aerosol liquid water (ALW) induced by the wet growth could play a significant role in the sulfate formation and emphasized the importance of bulk aqueous-phase oxidation of SO_2 in ALW and heterogeneous reaction of SO_2 on aerosol surfaces involving ALW. ALW also plays an important role in secondary organic aerosol (SOA) formation (Hastings et al., 2005; Healy et al., 2009; Kamens et al., 2011; Koehler et al., 2004). Numerous studies have investigated the effect of RH on SOA formed from different aromatics during their photochemical oxidation processes (Blando and Turpin, 2000; Cocker et al., 2001; Seinfeld et al., 2001; Zhou et al., 2011; Jia and Xu., 2014). Furthermore, Zhang et al. (2015) have revealed that, as the RH increases from 40% to 85% in the Yangtze River Delta of China, the aerosol scattering and backscattering coefficients increase by 58% and 25%, respectively, and the calculated aerosol direct radiative forcing caused by hygroscopic growth is increased by 47%.

In recent years, China has experienced persistent haze pollution with unprecedentedly high $PM_{2.5}$ concentrations during wintertime, particularly in North China Plain (NCP) (Chan and Yao, 2008; He et al., 2001; Kan et al., 2012; Guo et al., 2014; Wang et al., 2014; Fu et al., 2014). A conceptual model based on the aerosol radiation feedback (ARF) has been established to interpret the wintertime heavy haze formation, in which water vapor is considered to play a key role in the progressive accumulation and formation of $PM_{2.5}$. In winter, when the atmospheric condition is stagnant, air pollutants commence to accumulate in the planetary boundary layer (PBL), favorable for the $PM_{2.5}$ formation. Increasing $PM_{2.5}$ scatters or absorbs the incoming solar radiation to lower the surface temperature and cause anomalous temperature inversion, subsequently suppressing the vertical turbulent diffusion and decreasing the planetary boundary layer height (PBLH) to further trap more air pollutants

and water vapor to increase the RH in the PBL. Increasing RH enhances aerosol hygroscopic growth and multiphase reactions and augments the particle size and mass, causing further dimming and decrease of the surface temperature and PBL height (Quan et al., 2013; Tie et al., 2017; Ding et al., 2017). However, few studies have been performed in China to comprehensively quantify the effect of water vapor in the atmospheric physical and chemical process on the $PM_{2.5}$ pollution to further verify the haze formation.

The purpose of the present study is to quantitatively evaluate the contribution of aerosol water induced by the aerosol wet growth to $PM_{2.5}$ concentrations in NCP using the Weather Research and Forecast model with Chemistry (WRF-Chem). The model configuration and methodology are described in Section 2. Results and discussions are presented in Section 3, and conclusions and summaries are given in Section 4.

2 Model and methodology

2.1 WRF-Chem Model and Configuration

A persistent air pollution episode with high levels of $PM_{2.5}$ from 05 December 2015 to 04 January 2016 in NCP was simulated using the WRF-Chem model with modifications by Li et al. (2010, 2011a, b, 2012) from the Molina Center for Energy and the Environment. Figure 1 shows the WRF-Chem model simulation domain and Table 1 provides the model configurations. Detailed model description can be found in Wu et al. (2018a).

2.2 Data and Methodology

The model performance of RH was validated using the hourly measurements in Luancheng, Yucheng, and Jiaozhouwan observed from the Chinese Ecosystem Research Network (CERN). Furthermore, the NCEP reanalysis data was used to compare to the simulated RH distribution. The detailed information of other data used for validation can be found in Wu et al. (2018a).

The mean bias (*MB*), root mean square error (*RMSE*) and the index of agreement (*IOA*) were utilized to evaluate the performance of the WRF-Chem model simulations against measurements. To assess the contributions of ALW to the near-surface concentrations of air pollutants in NCP, the factor separation approach (FSA) was used in this study (Stein and Alpert, 1993; Gabusi et al., 2008; Li et al., 2014). Generally, the formation of the secondary atmospheric pollutants, such as O_3, secondary organic aerosol, and nitrate, is a complicated nonlinear process in which its precursors from various emissions sources and transport react chemically or reach equilibrium thermodynamically. Nevertheless, it is not straightforward to evaluate the contributions from different factors in a nonlinear process (Wu et al., 2017). The factor separation approach (FSA) proposed by Stein and Alpert (1993) can be used to isolate the effect of one single factor from a nonlinear process and has been widely used to evaluate source effects. The total effect of one factor in the presence of others can be decomposed into contributions from the factor and that from the interactions of all those factors. Considering that there are two factors *X* and *Y* that influence the formation of secondary pollutants in the atmosphere and also interact with each other. Denoting $\boldsymbol{f_{XY}}$, $\boldsymbol{f_X}$, $\boldsymbol{f_Y}$, and $\boldsymbol{f_0}$ as the simulations including both of two factors, factor *X* only, factor *Y* only, and none of the two factors, respectively. The contributions of factor *X* and *Y* can be defined as $\boldsymbol{f_{XY} - f_Y}$ and $\boldsymbol{f_{XY} - f_X}$, respectively. Detailed description of the methodology can be found in Wu et al. (2017).

3 Results and discussions

3.1 Relationship between RH and near-surface $PM_{2.5}$ concentrations

High RH has been suggested to be an important factor facilitating the SA formation in the atmosphere and aggravating the haze pollution (Sun et al., 2013; Cheng et al., 2015). Figure 2 presents the scatter plot of the near-surface $PM_{2.5}$ concentrations ([$PM_{2.5}$]) and RH in

149 the winter of 2015 at six typical polluted cities in NCP, including Beijing, Tianjin,
150 Shijiazhuang, Tangshan, Baoding, and Chengde. The observed near-surface [$PM_{2.5}$] at those
151 six cities display a growing trend with increasing RH, suggesting that the ALW induced by
152 the hygroscopic growth under high RH conditions has potentials to accelerate the $PM_{2.5}$
153 formation and accumulation. Increasing RH facilitates the aerosol hygroscopic growth and
154 further enhances the ALW, which serves as an efficient medium for promoting the
155 liquid-phase and heterogeneous reactions and accelerating the transformation of reactive
156 gaseous pollutants into the particle phase. Increased ALW also augments the particle size,
157 enhancing the ARF to increase the near-surface [$PM_{2.5}$]. However, the attenuation of
158 incoming solar radiation caused by the ALW also decreases the photolysis rates, unfavorable
159 for photochemical activities and lowering the atmospheric oxidation capability (AOC). Field
160 measurements show that large fraction of SA in $PM_{2.5}$ has been observed in NCP during
161 wintertime (Sun et al., 2013; Guo et al., 2014; Xu et al., 2015). Therefore, decreased AOC
162 generally does not facilitate the SA formation, particularly with regards to SOA and nitrate,
163 to partially counteract the $PM_{2.5}$ enhancement caused by the ALW. It is also worth noting that
164 since high RH frequently corresponds to atmospheric stagnation, near-surface [$PM_{2.5}$] also
165 build up under high RH conditions. For example, the humid air mass is subject to being
166 transported from south to NCP under the stagnant weather with weak south winds and
167 meanwhile the $PM_{2.5}$ also accumulates due to the unfavorable dispersion condition.
168 Additionally, when the RH is very high, there also exist the low near-surface [$PM_{2.5}$] shown
169 in Figure 2, demonstrating that other factors, such as emissions, horizontal transport, vertical
170 exchange, and precipitation, also substantially influence near-surface [$PM_{2.5}$]. Generally, high
171 occurrence frequency of precipitation coincides with high RH, thus the precipitation washout
172 might constitute one of the most possible reasons for the low near-surface [$PM_{2.5}$] under high
173 RH situations. Therefore, it is still imperative to verify quantitatively the contribution of the

174 ALW to near-surface [$PM_{2.5}$].

175 **3.2 Model validation**

176 The WRF-Chem model simulation of the haze pollution episode in NCP has been
177 comprehensively validated using available measurements in Wu et al. (2018a). In general, the
178 model simulates well the spatial distribution and temporal variation of $PM_{2.5}$, O_3, NO_2, SO_2
179 and CO mass concentrations compared to observations in NCP. The predicted aerosol species
180 are also in good agreement with the measurement in Beijing. Moreover, the model performs
181 reasonably well in simulating the aerosol optical depth and single scattering albedo, PBL
182 height and downward shortwave flux against measurements.

183 In order to verify the effect of the ALW on near-surface [$PM_{2.5}$] during the haze
184 pollution episode, the simulated temporal variation of RH was first compared to
185 measurements at Luancheng, Yucheng, and Jiaozhouwan in NCP from 05 December 2015 to
186 04 January 2016 (Figure 3). The WRF-Chem model generally performs well in simulating
187 the hourly variation of RH in these three cities, with *IOA*s of 0.73, 0.83, and 0.69,
188 respectively. RH is a key meteorological component, sensitive to the atmospheric
189 thermodynamic (e.g., temperature) and dynamic (e.g., winds) conditions. Even when the
190 simulated water vapor content is the same as the observation, the overestimation or
191 underestimation of temperature still causes underestimation or overestimation of RH. Biases
192 of wind speeds and directions considerably influence the origination of air mass at the
193 observation site. In general, the northerly wind carries dry air, and is opposite for the
194 southerly wind during wintertime in NCP. Therefore, the uncertainties from meteorological
195 field simulations might constitute one of the most possible reasons for the RH bias (Bei et al.,
196 2017). Figure 4 presents the pattern comparison of the average simulated RH and the NCEP
197 reanalysis during the episode. The simulated RH distribution is generally consistent with that
198 from the reanalysis, e.g., dry air in West China and fairly humid air in South China. However,

199 the air over NCP in the simulation is more humid than the analysis, and the average simulated
200 RH is 70.6%, about 20% higher than the reanalyzed RH, which might be caused by the
201 temperature decrease due to the ARF considered in the simulation.

202 **3.3 Sensitivity studies**

203 The ALW not only enlarges the particle size to increase the aerosol optical depth (AOD),
204 likely enhancing the ARF to facilitate the $PM_{2.5}$ accumulation or to alter photolysis rates to
205 affect the AOC, but also influences the SA formation serving as a medium for multiphase
206 reactions. Therefore, sensitivity studies are used to quantitatively evaluate the effect of the
207 ALW on the $PM_{2.5}$ concentration during the haze pollution episode.

208 The FSA method was used to evaluate the contribution of the ALW to near-surface
209 [$PM_{2.5}$] by differentiating two model simulations with and without the ALW effect. Besides
210 the base case with all the ALW effect (hereafter referred to as $\mathbf{f_{base}}$), additional four
211 sensitivity simulations have been performed, in which the ALW effect on the ARF,
212 photolysis, multiphase reactions, and the total is excluded, respectively (hereafter referred to
213 as $\mathbf{f_{alw\_rad0}}$, $\mathbf{f_{alw\_j0}}$, $\mathbf{f_{alw\_het0}}$, and $\mathbf{f_{alw\_tot0}}$, respectively). It is worth noting that in all the
214 sensitivity simulations, the aerosol hygroscopic growth is not turned off. In the sensitivity
215 simulation $\mathbf{f_{alw\_rad0}}$, only the ALW contribution to the AOD is not included in the ARF. In
216 the $\mathbf{f_{alw\_j0}}$, only the ALW contribution to the AOD is not considered in the photolysis
217 calculation. In the $\mathbf{f_{alw\_het0}}$, only the heterogeneous formation of secondary aerosols (SA)
218 involving the ALW is turned off, including the SO_2 heterogeneous oxidation by O_2 catalyzed
219 by Fe^{3+}, N_2O_5 heterogeneous hydrolysis, and the heterogeneous reaction of glyoxal and
220 methylglyoxal. For the $\mathbf{f_{alw\_tot0}}$, the ALW contribution to the AOD is not considered in the
221 ARF and photolysis calculation, and the SA heterogeneous formation involving the ALW is
222 excluded. Detailed description about the sensitivity simulations can be found in Table 2. The
223 difference between $\mathbf{f_{base}}$ and $\mathbf{f_{alw\_rad0}}$ represents the ALW effect on the ARF during the

224 study episode, and so does for the ALW effect on photochemistry, multiphase reactions, and
225 the total ALW effect.
226
227 **3.3.1 ALW effect on the ARF**
228 The ALW, caused by the aerosol hygroscopic growth, augments the particle size to
229 increase AOD, potentially enhancing the ARF and aggravating the haze pollution. Figure 5
230 shows the distribution of the average AOD contribution due to the ALW during the haze
231 episode, evaluated by differentiating f_{base} and f_{alw_rad0}. Apparently, the ALW
232 substantially increases the AOD in NCP, with the contribution ranging from 30% to more
233 than 50%, indicating that ALW is an important contributor of the AOD. Substantial increase
234 of the AOD due to the ALW is anticipated to attenuate the incoming solar radiation,
235 decreasing the surface temperature and suppressing the PBL development, therefore,
236 deteriorating the haze pollution, as proposed by recent studies (Tie et al., 2017; Liu et al.,
237 2018).
238 Figure 6 presents the distribution of the average near-surface $PM_{2.5}$ contribution of the
239 ALW effect on the ARF (hereafter referred as to ALW-ARF) during the haze episode.
240 Interestingly, the ALW-ARF does not increase the near-surface [$PM_{2.5}$] consistently in NCP,
241 as expected. The ALW-ARF enhances the near-surface [$PM_{2.5}$] most strikingly in the south of
242 Hebei, with a contribution of more than 15 μg m^{-3} (less than 7%). However, in some areas,
243 such as the east of Shandong, the near-surface $PM_{2.5}$ contribution of the ALW-ARF is
244 negative, or the ALW-ARF decreases [$PM_{2.5}$]. On average, the ALW-ARF increases
245 near-surface [$PM_{2.5}$] in NCP during the episode by about 1.1 μg m^{-3}, so cannot constitute an
246 important factor for the heavy haze formation.
247 It is worth noting that enlarged particles due to the ALW not only increase the AOD to
248 enhance aerosol backward scattering, but also cause the aerosol spectrum to successively

shift toward larger sizes. Based on the Mie scattering theory, when the particle size is similar to the wavelength of incoming solar radiation, the radiation is favored to be scattered in the forward directions. In order to further verify the ALW effect on solar radiation and near-surface [$PM_{2.5}$], an ensemble method is employed similar to that reported in Wu et al. (2018a). The daytime near-surface [$PM_{2.5}$] in NCP during the episode in $\boldsymbol{f_{base}}$ are first subdivided into 30 bins with the interval of 20 μg m^{-3}. The AOD at 550 nm, aerosol effective radius (Reff), downward shortwave radiation at the surface (SWDOWN), surface temperature (TSFC), PBLH, and near-surface [$PM_{2.5}$] in $\boldsymbol{f_{base}}$ and $\boldsymbol{f_{alw\_rad0}}$ in the same grid cell are assembled as the bin [$PM_{2.5}$], respectively, and an average of these variables in each bin are calculated. Figure 7 shows the variation of AOD and Reff in $\boldsymbol{f_{base}}$ and $\boldsymbol{f_{alw\_rad0}}$ as a function of bin [$PM_{2.5}$]. The ALW not only significantly enhances the AOD, with an average contribution of 46% in NCP during the episode, but also increases the Reff considerably (Figures 7a and 7b). The Reff enhancement due to the ALW is the most striking with near-surface [$PM_{2.5}$] between 40 and 160 μg m^{-3}, exceeding 60%. On average, the ALW increases the Reff from 0.31 μm to 0.48 μm, close to the peak band of solar radiation. Therefore, the ALW increases the AOD to scatter more incoming solar radiation, decreasing the SWDOWN, but augments particle sizes to favor the forward scattering, increasing the SWDOWN. Generally, the decrease of the SWDOWN caused by the ALW is not significant, less than 1% with near-surface [$PM_{2.5}$] less than 200 μg m^{-3} and ranging from 2% to 3% with [$PM_{2.5}$] exceeding 240 μg m^{-3} (Figure 8a). Correspondingly, the ALW-ARF effect on the daytime TSFC is also marginal and the TSFC is decreased by less than 0.2°C (Figure 8b). Furthermore, the ALW-ARF generally increases the daytime PBLH with near-surface [$PM_{2.5}$] less than 140 μg m^{-3}, but is opposite with [$PM_{2.5}$] exceeding 140 μg m^{-3} (Figure 8c). Hence, the contribution of the ALW-ARF to near-surface [$PM_{2.5}$] is highly uncertain (Figure 8d),

depending on the relative importance of the ALW induced enhancement of aerosol backward and forward scattering.

3.3.2 ALW effect on the photochemistry

In addition to the ARF, the ALW also exerts an impact on the photochemistry by altering the aerosol backward and forward scattering to affect the photolysis, further influencing the ozone (O_3) and SA formation. Previous studies have shown that the ALW modifies the vertical profile of photolysis rate of NO_2 ($\boldsymbol{J_{NO_2}}$), inhibiting it at the ground level and accelerating it in the upper PBL (Tao et al., 2014; Dickerson et al., 1997). The combination reaction between the ground state oxygen atom (O^3P), produced from NO_2 photolysis, and oxygen molecules (O_2) forms O_3, representing the only important source of O_3 in the troposphere:

$$\boldsymbol{NO_2 + h\nu \rightarrow NO + O(^3P)} \quad (1)$$

$$\boldsymbol{O(^3P) + O_2 + M \rightarrow O_3 + M} \quad (2)$$

Thus, the variation of $\boldsymbol{J_{NO_2}}$ considerably affects the O_3 formation in the troposphere, changing the AOC and further the SA formation.

Figures 9a and 9b present the distribution of the percentage variation of average daytime $\boldsymbol{J_{NO_2}}$ due to the ALW during the haze episode at the 1st and 5th model layer, respectively. At the 1st model layer, except in the north of Jiangsu, the ALW generally decreases $\boldsymbol{J_{NO_2}}$ slightly in NCP. However, at 5th model layer, the region with enhanced $\boldsymbol{J_{NO_2}}$ caused by the ALW is obviously increased compared to that at 1st model layer. Apparently, the ALW induced enlargement of particle sizes increases the AOD and enhances the aerosol backward scattering to reduce the solar radiation reaching the ground level, decreasing the photolysis rate, but the enhanced forward scattering still potentially accelerates the photolysis, such as in the north of Jiangsu. In addition, the enhanced aerosol backward scattering also increases the photolysis rate in the upper and above PBL, which is consistent with previous studies (Tao et

298 al., 2014; Dickerson et al., 1997). The variation of average daytime O_3 concentrations is not
299 consistent with that of J_{NO_2} at the 1st model layer (Figure 9c). For example, although the
300 J_{NO_2} is decreased in Hebei and Shandong, the O_3 concentration is still enhanced by the ALW
301 in some areas of the two provinces. One of the possible reasons is the vertical transport of O_3
302 from the upper layers where the O_3 is plausibly enhanced due to the increased photolysis rate
303 (Figure 9b). At the 5th model layer, the area with enhanced O_3 concentrations is much larger
304 than that at 1st model layer, which is in agreement with the variation of the J_{NO_2} (Figure 9d).
305 On average, the ALW decreases near-surface (1st model layer) daytime O_3 concentrations by
306 about 0.2 μg m^{-3} (or 0.45%), playing a minor role in O_3 formation.

307 Figure 10 shows the distribution of the average near-surface $PM_{2.5}$ contribution of the
308 ALW effect on the photolysis frequencies (hereafter referred as to ALW-J) during the haze
309 episode. Except in some areas in Shandong and Anhui, the ALW-J slightly decreases
310 near-surface [$PM_{2.5}$] in NCP, with an average reduction of about 0.87 μg m^{-3} (or 0.64%).
311 Therefore, the ALW-J does not play an important role in mitigating the haze pollution.

312 **3.3.3 ALW effect on heterogeneous reactions**

313 The ALW provides an excellent substrate for heterogeneous reactions in the atmosphere,
314 which has been proposed to play a key role in the SA formation during haze days (Li et al.,
315 2017; Xing et al., 2018).

316 Figure 11 presents the distribution of contributions of the ALW on heterogeneous
317 reactions (hereafter referred to ALW-HET) to near-surface sulfate, nitrate, and ammonium
318 concentrations averaged during the haze episode. A parameterization of sulfate
319 heterogeneous formation involving ALW has been developed and implemented into the
320 WRF-Chem model, which has successfully reproduced the observed rapid sulfate formation
321 during haze days (Li et al., 2017). The sulfate heterogeneous formation from SO_2 is
322 parameterized as a first order irreversible uptake by ALW surfaces, with a reactive uptake

coefficient of 0.5×10^{-4} assuming that there is enough alkalinity to maintain the high iron-catalyzed reaction rate. The contribution of the ALW-HET to the sulfate formation is substantial in NCP, exceeding 5 μg m^{-3} (or 50%) in NCP (Figures 11a and 11b). The ALW-HET contributes about 71.3% of the sulfate in NCP during the episode, indicating that the heterogeneous formation involving the ALW is the dominant sulfate source during haze days.

The heterogeneous hydrolysis of N_2O_5 on the surface of deliquescent aerosols leads to the HNO_3 formation, which is the key contributor to the nitrate aerosol loading (Riemer et al., 2003; Pathak et al., 2011; Chang et al., 2016). In this study, the parameterization of the heterogeneous hydrolysis of N_2O_5, proposed by Riemer et al. (2003), has been included in the WRF-Chem model for considering the effect of ALW-HET on the nitrate formation. The N_2O_5 uptake coefficient on wet aerosol surfaces ranges from 0.002 to 0.02, depending on the sulfate and nitrate aerosol mass. The ALW-HET generally increases the near-surface nitrate mass concentration by 2 to 8 μg m^{-3} in NCP, with an average contribution of 2.8 μg m^{-3} (or 10%) (Figures 11c and 11d). It is worth noting that the ALW-HET does not consistently increase the nitrate formation and the nitrate concentration is considerably decreased in some areas in east China. One of the possible reasons is that the ALW-HET substantially enhances the sulfate formation and the increased sulfate competes with nitrate for ammonia (NH_3), suppressing the nitrate formation. Figure 12 shows the distribution of the NH_3 emission rate in December. High NH_3 emissions are concentrated in NCP, Central China, Sichuan basin, and Northeast China, where the nitrate concentration is generally increased by the ALW-HET.

Ammonium serves as the main alkali in the atmosphere to neutralize acidic aerosols such as sulfate and nitrate, so its formation is not only dependent on its precursor (NH_3), but is also influenced by acid aerosols. The ALW-HET enhances the near-surface ammonium

mass concentration most strikingly in NCP with high NH_3 emissions and increased sulfate and nitrate aerosols. The contribution of the ALW-HET to the ammonium concentration varies from 2 to more than 10 μg m^{-3}, with an average of 4.2 μg m^{-3} (or 25.6%), showing that the heterogeneous formation constitutes an important ammonium source (Figures 11e and 11f).

Heterogeneous reactions are also an important pathway for the SOA formation (Fu et al., 2008; Li et al., 2013). Laboratory and field studies have indicated that glyoxal and methylglyoxal play an important role in SOA formation via aerosol uptake or cloud processing (Liggio et al., 2005; Volkamer et al., 2007; Li et al., 2011). In this study, the heterogeneous reaction of SOA formation from glyoxal and methylglyoxal is parameterized as a first-order irreversible uptake by aerosol particles, with a reaction uptake coefficient of 3.7×10^{-3} (Liggio et al., 2005; Zhao et al., 2006; Volkamer et al., 2007; Li et al., 2011). During the haze episode, the average near-surface SOA contribution of the ALW-HET is 7.4 μg m^{-3} (or 48%) in NCP, ranging from 3 to over 15 μg m^{-3} (or 30 to over 50%) in NCP, showing that heterogeneous reactions of glyoxal and methylglyoxal on wet aerosol surfaces play a critical role in SOA formation (Figure 13). Xing et al. (2018) have demonstrated that, in Beijing-Tianjin-Hebei, the near-surface SOA contribution from glyoxal and methylglyoxal is around 30% during a haze episode in January 2014, much less than that (48%) in the study. The possible reason is that the RH in the episode is higher than that in Xing et al. (2018), causing more SOA formation from glyoxal and methylglyoxal.

High SA contribution to the haze pollution has been observed in China (e.g., Huang et al., 2014), so the ALW-HET substantially enhances the SA formation, constituting an important factor for heavy haze formation. Figure 14 shows the contribution of the ALW-HET to average near-surface [$PM_{2.5}$] during the study episode. The ALW-HET enhances near-surface [$PM_{2.5}$] by more than 40 μg m^{-3} in the central part of NCP, and on

373 average, the $PM_{2.5}$ contribution of the ALW-HET is 21.7 μg m^{-3} (or 15.9%), less than the
374 total enhancement of 25.1 μg m^{-3} (or 18.4%) from sulfate, nitrate, ammonium, and SOA. The
375 inconsistency indicates that the ALW-HET induced SA enhancement causes a decrease in
376 primary aerosols. Figure 15a and 15b show the percentage decrease of black carbon (BC) and
377 primary organic aerosols (POA) as a function of bin [$PM_{2.5}$], respectively. Interestingly, the
378 average BC and POA concentrations are decreased by 5.1% and 5.2% due to the ALW-HET,
379 respectively. The ALW-HET induced SA enhancement augment the particle size and should
380 increase the AOD. However, on the contrary, the ALW-HET decreases the AOD, although
381 considerably increases the Reff (Figures 16a and 16b). The reason is that the enhanced SA
382 enlarges particle sizes, facilitating the coagulation to decrease the aerosol number
383 concentration and surface area, as shown in Figures 16c and 16d. Hence, the decreased AOD
384 and increased Reff due to the ALW-HET enhance the SWDOWN and TSFC, further
385 increasing the PBLH and decreasing near-surface primary aerosols, as shown in Figure 17.

386 It is worth noting that the ALW content (ALWC) and aerosol composition are mutually
387 influenced, i.e., the ALWC depends on the existence of hydroscopic aerosols (mainly
388 inorganic components) and the RH in the atmosphere, and the SA, particularly inorganic
389 components, formed via heterogeneous and aqueous reactions involving the ALW further
390 increases the ALWC. Hence the initial hydroscopic aerosols might play a seeding role in the
391 contribution of the ALW-HET, likely constituting the most important factor in determining
392 the ALWC and additional SA formed via heterogeneous or aqueous reactions. However, in
393 model simulations, the initial hydroscopic aerosols or the seed particles, are insignificant to
394 the ALWC, since even without consideration of multiphase formation, the other processes
395 still dominate the hydroscopic aerosol concentration in the atmosphere, including direct
396 emissions, nucleation, condensation et al., particularly after model spin-up. Therefore, the
397 effect of initial hydroscopic aerosols or seed particles on the ALW and additional

heterogeneous SA is generally negligible.

3.3.4 ALW total effect

Above discussions have shown that the ALW influences near-surface [$PM_{2.5}$] through complicated physical and chemical processes, which interact with each other. Figure 18 shows the near-surface $PM_{2.5}$ contribution of the total ALW effect (hereafter referred as to ALW-TOT) during the haze episode, evaluated by differentiating f_{base} and f_{alw_tot0}. The ALW-TOT plays an important role in the $PM_{2.5}$ formation during the wintertime haze pollution in NCP, with an average contribution of 23.8 μg m^{-3} (or 17.5%), ranging from 5 to over 40 μg m^{-3}. About 78% of the enhanced near-surface [$PM_{2.5}$] due to the ALW-TOT is contributed by secondary inorganic aerosols, in which the contributions from sulfate, nitrate, and ammonium are 45%, 14% and 19%, respectively, and around 32% is contributed by SOA. Therefore, about 10% of near-surface [$PM_{2.5}$] enhancement from SA is counterbalanced by the decrease in the primary aerosols. Therefore, the ALW induced enhancement of near-surface [$PM_{2.5}$] is overwhelmingly determined by the ALW-HET, and the ALW-ARF and ALW-J are subject to decreasing [$PM_{2.5}$].

Figure 19 shows the variation of near-surface [$PM_{2.5}$] caused by the ALW-TOT, ALW-HET, ALW-ARF, and ALW-J, respectively, as a function of bin near-surface RH in NCP during the haze episode to further assess the ALW effect. The hourly near-surface RH in f_{base} is first divided into 28 bins, ranging from 30% to 100%, with interval of 2.5%. The $PM_{2.5}$ contribution from the four sensitivity simulations is assembled in the same grid cell as the bin RH, and an average of $PM_{2.5}$ contribution in each bin is calculated. The ALW does not continuously increase near-surface [$PM_{2.5}$] with the RH. When the RH is less than 80%, the near-surface $PM_{2.5}$ contribution of the ALW-TOT generally increases rapidly with the RH. However, when the RH exceeds 80%, the contribution commences to decrease and fluctuates between 20 and 30 μg m^{-3}, showing the effect of high occurrence frequencies of precipitation.

In addition, the ALW-HET dominates the $PM_{2.5}$ contribution, particularly with RH less than 50%. The ALW-RAD generally decreases [$PM_{2.5}$] slightly with the RH less than 52.5% and vice versa with the RH more than 52.5%. The $PM_{2.5}$ contribution of the ALW-J is negative and less than 1.5 μg m^{-3}, except when the RH is between 92.5% and 97.5%.

4 Conclusions and summaries

The good relationships between near-surface [$PM_{2.5}$] concentration and RH during the wintertime of 2015 in NCP indicate the possibility that high RH plays an important role in the $PM_{2.5}$ formation during the haze pollution. A severe haze pollution episode from 05 December 2015 to 04 January 2016 is simulated using the WRF-Chem model to investigate the impact of ALW caused by the accumulated moisture on near surface [$PM_{2.5}$] in NCP. The air over NCP during the haze episode is humid, with an average simulated RH of about 71%. In general, the WRF-Chem model reproduces reasonably well the temporal variations of RH compared to observations at three sites in NCP, although the model biases still exist due to the uncertainties in simulated meteorological fields.

The FSA method is used to evaluate the contribution of the ALW effect on ARF, photochemistry and heterogeneous reactions to the wintertime $PM_{2.5}$ concentration in NCP. Model results show that the ALW substantially increases the daytime AOD with an average contribution of 46% in NCP during the episode, enhancing the aerosol backward scattering, and also augments the Reff from 0.31 μm to 0.48 μm, approaching the peak band of solar radiation, favoring the aerosol forward scattering. The ALW does not significantly attenuate the incoming solar radiation at the ground surface to enhance the ARF, and the average near-surface $PM_{2.5}$ contribution of the ALW-ARF is about 1.1 μg m^{-3} in NCP during the episode. Therefore, the ALW-ARF is not an important factor for heavy haze formation and its contribution relies on the relative importance of the ALW induced enhancement of aerosol

backward and forward scattering. The ALW generally decreases the photolysis rate at the surface level due to enhanced backward aerosol scattering, but the favored forward scattering still possibly accelerates the photolysis. Additionally, the ALW increases the photolysis rate in the upper and above PBL. On average, the ALW decreases near-surface daytime O_3 concentrations by 0.20 μg m^{-3} and [$PM_{2.5}$] by 0.87 μg m^{-3}, playing a minor role in mitigating the haze pollution.

The ALW substantially enhances the SA formation by serving as an important medium for liquid-phase and heterogeneous reactions. The ALW contribution to near-surface sulfate, nitrate, ammonium, and SOA concentrations is 71%, 10%, 26%, and 48% in NCP during the episode, respectively. However, the enhanced SA due to the ALW-HET enlarges particle sizes to facilitate the coagulation, decreasing the aerosol number concentration and surface area and further AOD. Therefore, the decreased AOD and increased Reff enhance the incoming solar radiation reaching the ground surface, further increasing the surface temperature and PBLH and decreasing near-surface primary aerosols. The ALW-HET contributes 15.9% of near-surface [$PM_{2.5}$], less than the total SA enhancement of 18.4%, and the rest is counterbalanced by the decrease in primary aerosols.

The near-surface $PM_{2.5}$ contribution of the ALW total effect is 17.5% in NCP, indicating that ALW plays an important role in the $PM_{2.5}$ formation during the wintertime haze pollution. Moreover, the ALW-HET overwhelmingly dominates the $PM_{2.5}$ enhancement due to the ALW. The ALW does not consistently enhance near-surface [$PM_{2.5}$] with increasing RH. When the RH exceeds 80%, the contribution of the ALW commences to decrease caused by the high occurrence frequencies of precipitation.

Although the model performs reasonably well in simulating air pollutants, aerosol species and optical properties, and RH during the episode in NCP, the uncertainties from meteorological fields and emission inventory still exist, leading to model biases. In addition,

simulation period of one month might not be sufficient to provide a comprehensive view of the ALW effect on the $PM_{2.5}$ formation. More wintertime case studies will need to be performed in the future to further investigate the ALW effect.

Author contribution. Guohui Li, as the contact author, provided the ideas and financial support, developed the model code, verified the conclusions, and revised the paper. Jiarui Wu conducted a research, designed the experiments, carried the methodology out, performed the simulation, processed the data, prepared the data visualization, and prepared the manuscript with contributions from all authors. Naifang Bei provided the treatment of meteorological data, analyzed the study data, validated the model performance, and reviewed the manuscript. Bo Hu provided the observation data used in the study, synthesized the observation, and reviewed the paper. Suixin Liu, Meng Zhou, Qiyuan Wang, Zirui Liu, and Yichen Wang provided the data and the primary data process, and reviewed the manuscript. Xia Li, Lang Liu, and Tian Feng analyzed the initial simulation data, visualized the model results and reviewed the paper. Junji Cao, Xuexi Tie, Jun Wang provided critical reviews pre-publication stage. Luisa T. Molina provided a critical preview and financial support, and revised the manuscript.

Acknowledgements. This work is financially supported by the National Key R&D Plan (Quantitative Relationship and Regulation Principle between Regional Oxidation Capacity of Atmospheric and Air Quality (2017YFC0210000)) and National Research Program for Key Issues in Air Pollution Control (DQGG0105). Luisa Molina acknowledges support from US NSF Award 1560494.

Reference

Ackerman, T., and Baker, M. B.: Shortwave radiative effects of unactivated aerosol-particles in clouds, J. Appl. Meteorol., 16, 63-69, 10.1175/1520-0450(1977)016<0063:sreoua>2.0.co;2, 1977.

Ackerman, T. P.: Model of effect of aerosols on urban climates with particular applications to Los-angeles basin, J. Atmos. Sci., 34, 531-547, 10.1175/1520-0469(1977)034<0531:amoteo>2.0.co;2, 1977.

Bei, N. F., Li, G. H., Huang, R. J., Cao, J. J., Meng, N., Feng, T., Liu, S. X., Zhang, T., Zhang, Q., and Molina, L. T.: Typical synoptic situations and their impacts on the wintertime air pollution in the Guanzhong basin, China, Atmos. Chem. Phys., 16, 7373-7387, 10.5194/acp-16-7373-2016, 2016a.

Bei, N. F., Xiao, B., Meng, N., and Feng, T.: Critical role of meteorological conditions in a persistent haze episode in the Guanzhong basin, China, Sci. Total Environ., 550, 273-284, 10.1016/j.scitotenv.2015.12.159, 2016b.

Bei, N. F., Wu, J. R., Elser, M., Feng, T., Cao, J. J., El-Haddad, I., Li, X., Huang, R. J., Li, Z. Q., Long, X., Xing, L., Zhao, S. Y., Tie, X. X., Prevot, A. S. H., and Li, G. H.: Impacts of meteorological uncertainties on the haze formation in Beijing-Tianjin-Hebei (BTH) during wintertime: a case study, Atmos. Chem. Phys., 17, 14579-14591, 10.5194/acp-17-14579-2017, 2017.

Blando, J. D., and Turpin, B. J.: Secondary organic aerosol formation in cloud and fog droplets: a literature evaluation of plausibility, Atmos. Environ., 34, 1623-1632, 10.1016/s1352-2310(99)00392-1, 2000.

Carrico, C. M., Kus, P., Rood, M. J., Quinn, P. K., and Bates, T. S.: Mixtures of pollution, dust, sea salt, and volcanic aerosol during ACE-Asia: Radiative properties as a function of relative humidity, J. Geophys. Res.-Atmos., 108, 18, 10.1029/2003jd003405, 2003.

Chan, C. K. and Yao, X.: Air pollution in mega cities in China, Atmos. Environ., 42, 1–42, 2008.

Chang, W. L., Brown, S. S., Stutz, J., Middlebrook, A. M., Bahreini, R., Wagner, N. L., Dube, W. P., Pollack, I. B., Ryerson, T. B., and Riemer, N.: Evaluating N_2O_5 heterogeneous hydrolysis parameterizations for CalNex 2010, J. Geophys. Res.-Atmos., 121, 5051-5070, 10.1002/2015jd024737, 2016.

Chen, F. and Dudhia, J.: Coupling an advanced land surface-hydrology model with the Penn State-NCAR MM5 modeling system. Part I: Model implementation and sensitivity, Mon. Weather Rev., 129(4), 569-585, 2001.

Cheng, Y., He, K. B., Du, Z. Y., Zheng, M., Duan, F. K., and Ma, Y. L.: Humidity plays an important role in the $PM_{2.5}$ pollution in Beijing, Environ. Pollut., 197, 68-75, 10.1016/j.envpol.2014.11.028, 2015.

Cheng, Y. F., Wiedensohler, A., Eichler, H., Heintzenberg, J., Tesche, M., Ansmann, A., Wendisch, M., Su, H., Althausen, D., Herrmann, H., Gnauk, T., Bruggemann, E., Hu, M., and Zhang, Y. H.: Relative humidity dependence of aerosol optical properties and

direct radiative forcing in the surface boundary layer at Xinken in Pearl River Delta of China: An observation based numerical study, Atmos. Environ., 42, 6373-6397, 10.1016/j.atmosenv.2008.04.009, 2008.

Chou, M.-D. and Suarez, M. J.: A solar radiation parameterization for atmospheric studies, NASA Tech. Rep. NASA/TM-1999- 10460, 15, 38 pp., 1999.

Chou, M.-D. and Suarez, M. J.: A thermal infrared radiation parameterization for atmospheric studies, NASA/TM-2001-104606, 19, 55 pp., 2001.

Cocker, D. R., Clegg, S. L., Flagan, R. C., and Seinfeld, J. H.: The effect of water on gas-particle partitioning of secondary organic aerosol. Part I: alpha-pinene/ozone system, Atmos. Environ., 35, 6049-6072, 10.1016/s1352-2310(01)00404-6, 2001a.

Cocker, D. R., Flagan, R. C., and Seinfeld, J. H.: State-of-the-art chamber facility for studying atmospheric aerosol chemistry, Environ. Sci. Technol., 35, 2594-2601, 10.1021/es0019169, 2001b.

Cocker, D. R., Mader, B. T., Kalberer, M., Flagan, R. C., and Seinfeld, J. H.: The effect of water on gas-particle partitioning of secondary organic aerosol: II. m-xylene and 1,3,5-trimethylbenzene photooxidation systems, Atmos. Environ., 35, 6073-6085, 10.1016/s1352-2310(01)00405-8, 2001c.

Covert, D. S., Charlson, R. J., and Ahlquist, N. C.: A Study of the Relationship of Chemical Composition and Humidity to Light Scattering by Aerosols, J. Appl. Meteorol., 11, 968-976, 1972.

Dickerson, R. R., Kondragunta, S., Stenchikov, G., Civerolo, K. L., Doddridge, B. G., and Holben, B. N.: The impact of aerosols on solar ultraviolet radiation and photochemical smog, Science, 278, 827-830, 10.1126/science.278.5339.827, 1997.

Ding, Y. H., Wu, P., Liu, Y. J., and Song, Y. F.: Environmental and Dynamic Conditions for the Occurrence of Persistent Haze Events in North China, Engineering, 3, 266-271, 10.1016/j.eng.2017.01.009, 2017.

Flocas, H., Kelessis, A., Helmis, C., Petrakakis, M., Zoumakis, M., and Pappas, K.: Synoptic and local scale atmospheric circulation associated with air pollution episodes in an urban Mediterranean area, Theo. Appl. Climatol., 95, 265-277, 10.1007/s00704-008-0005-9, 2009.

Fu, G. Q., Xu, W. Y., Yang, R. F., Li, J. B., and Zhao, C. S.: The distribution and trends of fog and haze in the North China Plain over the past 30 years, Atmos. Chem. Phys., 14, 11949-11958, 10.5194/acp-14-11949-2014, 2014.

Fu, T. M., Jacob, D. J., Wittrock, F., Burrows, J. P., Vrekoussis, M., and Henze, D. K.: Global budgets of atmospheric glyoxal and methylglyoxal, and implications for formation of secondary organic aerosols, J. Geophys. Res.-Atmos., 113, 17, 10.1029/2007jd009505, 2008.

Gabusi, V., Pisoni, E., and Volta, M.: Factor separation in air quality simulations, Ecol. Model., 218, 383-392, 10.1016/j.ecolmodel.2008.07.030, 2008.

Guenther, A., Karl, T., Harley, P., Wiedinmyer, C., Palmer, P. I., and Geron, C.: Estimates of global terrestrial isoprene emissions using MEGAN (Model of Emissions of Gases and Aerosols from Nature), Atmos. Chem. Phys., 6, 3181-3210, https://doi.org/10.5194/acp-6-3181-2006, 2006.

582 Guo, S., Hu, M., Zamora, M. L., Peng, J. F., Shang, D. J., Zheng, J., Du, Z. F., Wu, Z., Shao,
583 M., Zeng, L. M., Molina, M. J., and Zhang, R. Y.: Elucidating severe urban haze
584 formation in China, P. Natl. Acad. Sci. USA., 111, 17373-17378,
585 10.1073/pnas.1419604111, 2014.

586 Hallquist, M., Wenger, J. C., Baltensperger, U., Rudich, Y., Simpson, D., Claeys, M.,
587 Dommen, J., Donahue, N. M., George, C., Goldstein, A. H., Hamilton, J. F., Herrmann,
588 H., Hoffmann, T., Iinuma, Y., Jang, M., Jenkin, M. E., Jimenez, J. L., Kiendler-Scharr,
589 A., Maenhaut, W., McFiggans, G., Mentel, T. F., Monod, A., Prevot, A. S. H., Seinfeld,
590 J. H., Surratt, J. D., Szmigielski, R., and Wildt, J.: The formation, properties and impact
591 of secondary organic aerosol: current and emerging issues, Atmos. Chem. Phys., 9,
592 5155-5236, 10.5194/acp-9-5155-2009, 2009.

593 Hastings, W. P., Koehler, C. A., Bailey, E. L., and De Haan, D. O.: Secondary organic
594 aerosol formation by glyoxal hydration and oligomer formation: Humidity effects and
595 equilibrium shifts during analysis, Environ. Sci. Technol., 39, 8728-8735,
596 10.1021/es050446l, 2005.

597 He, K. B., Yang, F. M., Ma, Y. L., Zhang, Q., Yao, X. H., Chan, C. K., Cadle, S., Chan, T.,
598 and Mulawa, P.: The characteristics of $PM_{2.5}$ in Beijing, China, Atmos. Environ., 35,
599 4959-4970, 10.1016/s1352-2310(01)00301-6, 2001.

600 Healy, R. M., Temime, B., Kuprovskyte, K., and Wenger, J. C.: Effect of Relative Humidity
601 on Gas/Particle Partitioning and Aerosol Mass Yield in the Photooxidation of p-Xylene,
602 Environ. Sci. Technol., 43, 1884-1889, 10.1021/es802404z, 2009.

603 Hong, S.-Y. and Lim, J.-O. J.: The WRF Single-Moment 6-Class Microphysics Scheme
604 (WSM6), Asia-Pacific J. Atmos. Sci., 42, 129-151, 2006.

605 Horowitz, L. W., Walters, S., Mauzerall, D. L., Emmons, L. K., Rasch, P. J., Granier, C., Tie,
606 X. X., Lamarque, J. F., Schultz, M. G., Tyndall, G. S., Orlando, J. J., and Brasseur, G. P.:
607 A global simulation of tropospheric ozone and related tracers: Description and
608 evaluation of MOZART, version 2, J. Geophys. Res.-Atmos., 108, 4784,
609 https://doi.org/10.1029/2002jd002853, 2003.

610 Huang, R.-J., Zhang, Y., Bozzetti, C., Ho, K.-F., Cao, J.-J., Han, Y., Daellenbach, K. R.,
611 Slowik, J. G., Platt, S. M., Canonaco, F., Zotter, P., Wolf, R., Pieber, S. M., Bruns, E. A.,
612 Crippa, M., Ciarelli, G., Piazzalunga, A., Schwikowski, M., Abbaszade, G.,
613 Schnelle-Kreis, J., Zimmermann, R., An, Z., Szidat, S., Baltensperger, U., El Haddad, I.,
614 and Prévôt, A. S. H.: High secondary aerosol contribution to particulate pollution during
615 haze events in China, Nature, 514, 218-222, doi: 10.1038/nature13774, 2014.

616 Im, J. S., Saxena, V. K., and Wenny, B. N.: An assessment of hygroscopic growth factors for
617 aerosols in the surface boundary layer for computing direct radiative forcing, J. Geophys.
618 Res.-Atmos., 106, 20213-20224, 10.1029/2000jd000152, 2001.

619 Jacobson, M. Z.: Studying the effects of aerosols on vertical photolysis rate coefficient and
620 temperature profiles over an urban airshed, J. Geophys. Res.-Atmos., 103, 10593-10604,
621 10.1029/98jd00287, 1998.

622 Jacobson, M. Z.: Analysis of aerosol interactions with numerical techniques for solving
623 coagulation, nucleation, condensation, dissolution, and reversible chemistry among
624 multiple size distributions, J. Geophys. Res.-Atmos., 107, 23, 10.1029/2001jd002044,
625 2002.

626 Janjić, Z. I.: Nonsingular Implementation of the Mellor -Yamada Level 2.5 Scheme in the

627 NCEP Meso Model, Ncep Office Note, 436, 2002.

628 Jia, L., and Xu, Y. F.: Effects of Relative Humidity on Ozone and Secondary Organic
629 Aerosol Formation from the Photooxidation of Benzene and Ethylbenzene, Aerosol Sci.
630 Technol., 48, 1-12, 10.1080/02786826.2013.847269, 2014.

631 Kamens, R. M., Zhang, H. F., Chen, E. H., Zhou, Y., Parikh, H. M., Wilson, R. L., Galloway,
632 K. E., and Rosen, E. P.: Secondary organic aerosol formation from toluene in an
633 atmospheric hydrocarbon mixture: Water and particle seed effects, Atmos. Environ., 45,
634 2324-2334, 10.1016/j.atmosenv.2010.11.007, 2011.

635 Kan, H. D., Chen, R. J., and Tong, S. L.: Ambient air pollution, climate change, and
636 population health in China, Environ. Int., 42, 10-19, 10.1016/j.envint.2011.03.003,
637 2012.

638 Koehler, C. A., Fillo, J. D., Ries, K. A., Sanchez, J. T., and De Haan, D. O.: Formation of
639 secondary organic aerosol by reactive condensation of furandiones, aldehydes, and
640 water vapor onto inorganic aerosol seed particles, Environ. Sci. Technol., 38, 5064-5072,
641 10.1021/es034672b, 2004.

642 Kurokawa, J., Ohara, T., Morikawa, T., Hanayama, S., Janssens- Maenhout, G., Fukui, T.,
643 Kawashima, K., and Akimoto, H.: Emissions of air pollutants and greenhouse gases over
644 Asian regions during 2000–2008: Regional Emission inventory in Asia (REAS) version
645 2, Atmos. Chem. Phys., 13, 11019–11058, https://doi.org/10.5194/acp-13-11019-2013,
646 2013.

647 Li, G., Lei, W., Zavala, M., Volkamer, R., Dusanter, S., Stevens, P., and Molina, L. T.:
648 Impacts of HONO sources on the photochemistry in Mexico City during the
649 MCMA-2006/MILAGO Campaign, Atmos. Chem. Phys., 10, 6551-6567,
650 10.5194/acp-10-6551-2010, 2010.

651 Li, G., Bei, N., Tie, X., and Molina, L. T.: Aerosol effects on the photochemistry in Mexico
652 City during MCMA-2006/MILAGRO campaign, Atmos. Chem. Phys., 11, 5169-5182,
653 10.5194/acp-11-5169-2011, 2011a.

654 Li, G., Zavala, M., Lei, W., Tsimpidi, A. P., Karydis, V. A., Pandis, S. N., agaratna, M. R.,
655 and Molina, L. T.: Simulations of organic aerosol concentrations in Mexico City using
656 the WRF-CHEM model during the MCMA-2006/MILAGRO campaign, Atmos. Chem.
657 Phys., 11, 3789-3809, 10.5194/acp-11-3789-2011, 2011b.

658 Li, G., Lei, W., Bei, N., and Molina, L. T.: Contribution of garbage burning to chloride and
659 $PM_{2.5}$ in Mexico City, Atmos. Chem. Phys., 12, 8751-8761, 10.5194/acp-12-8751-2012,
660 2012.

661 Li, G. H., Bei, N. F., Zavala, M., and Molina, L. T.: Ozone formation along the California
662 Mexican border region during Cal-Mex 2010 field campaign, Atmos. Environ., 88,
663 370-389, 10.1016/j.atmosenv.2013.11.067, 2014.

664 Li, G., Bei, N., Cao, J., Huang, R., Wu, J., Feng, T., Wang, Y., Liu, S., Zhang, Q., Tie, X.,
665 and Molina, L. T.: A possible pathway for rapid growth of sulfate during haze days in
666 China, Atmos. Chem. Phys., 17, 3301–3316, https://doi.org/10.5194/acp- 17-3301-2017,
667 2017a.

668 Li, N., Fu, T. M., Cao, J. J., Lee, S. C., Huang, X. F., He, L. Y., Ho, K. F., Fu, J. S., and Lam,
669 Y. F.: Sources of secondary organic aerosols in the Pearl River Delta region in fall:

Contributions from the aqueous reactive uptake of dicarbonyls, Atmos. Environ., 76, 200-207, 10.1016/j.atmosenv.2012.12.005, 2013.

Liggio, J., Li, S. M., and McLaren, R.: Reactive uptake of glyoxal by particulate matter, J. Geophys. Res.-Atmos., 110, doi: 10.1029/2004jd005113, 2005.

Liu, Q., Jia, X. C., Quan, J. N., Li, J. Y., Li, X., Wu, Y. X., Chen, D., Wang, Z. F., and Liu, Y. G.: New positive feedback mechanism between boundary layer meteorology and secondary aerosol formation during severe haze events, Sci. Rep., 8, 8, 10.1038/s41598-018-24366-3, 2018.

Nguyen, T. B., Roach, P. J., Laskin, J., Laskin, A., and Nizkorodov, S. A.: Effect of humidity on the composition of isoprene photooxidation secondary organic aerosol, Atmos. Chem. Phys., 11, 6931-6944, 10.5194/acp-11-6931-2011, 2011.

Parrish, D. D. and Zhu, T.: Clean Air for Megacities, Science, 326, 674–675, https://doi.org/10.1126/science.1176064, 2009.

Pathak, R. K., Wang, T., and Wu, W. S.: Nighttime enhancement of $PM_{2.5}$ nitrate in ammonia-poor atmospheric conditions in Beijing and Shanghai: Plausible contributions of heterogeneous hydrolysis of N_2O_5 and HNO_3 partitioning, Atmos. Environ., 45, 1183-1191, 10.1016/j.atmosenv.2010.09.003, 2011.

Penner, J. E., Hegg, D., and Leaitch, R.: Unraveling the role of aerosols in climate change, Environ. Sci. Technol., 35, 332A-340A, 10.1021/es0124414, 2001.

Poulain, L., Wu, Z., Petters, M. D., Wex, H., Hallbauer, E., Wehner, B., Massling, A., Kreiden- weis, S. M., and Stratmann, F.: Towards closing the gap between hygroscopic growth and CCN activation for secondary organic aerosols - Part 3: Influence of the chemical compo- sition on the hygroscopic properties and volatile fractions of aerosols, Atmos. Chem. Phys., 10, 3775–3785, doi:10.5194/acp-10-3775-2010, 2010.

Pilinis, C., Seinfeld, J. H., and Grosjean, D.: Water content of atmospheric aerosols, Atmos. Environ., 23, 1601–1606, 1989.

Quan, J. N., Gao, Y., Zhang, Q., Tie, X. X., Cao, J. J., Han, S. Q., Meng, J. W., Chen, P. F., and Zhao, D. L.: Evolution of planetary boundary layer under different weather conditions, and its impact on aerosol concentrations, Particuology, 11, 34-40, 10.1016/j.partic.2012.04.005, 2013.

Randles, C. A., Russell, L. M., and Ramaswamy, V.: Hygroscopic and optical properties of organic sea salt aerosol and consequences for climate forcing, Geophys. Res. Lett., 31, 4, 10.1029/2004gl020628, 2004.

Riemer, N., Vogel, H., Vogel, B., Schell, B., Ackermann, I., Kessler, C., and Hass, H.: Impact of the heterogeneous hydrolysis of N_2O_5 on chemistry and nitrate aerosol formation in the lower troposphere under photosmog conditions, J. Geophys. Res.-Atmos., 108, 21, 10.1029/2002jd002436, 2003.

Seinfeld, J. H., Erdakos, G. B., Asher, W. E., and Pankow, J. F.: Modeling the formation of secondary organic aerosol (SOA). 2. The predicted effects of relative humidity on aerosol formation in the alpha-pinene-, beta-pinene-, sabinene-, Delta(3)-Carene-, and cyclohexene-ozone systems, Environ. Sci. Technol., 35, 1806-1817, 10.1021/es001765+, 2001.

712 Seinfeld, J. H. and Pandis, S. N.: Atmospheric Chemistry and Physics: From Air Pollution to
713 Climate Change, John Wiley & Sons, USA, 1986.

714 Sun, Y., Wang, Z., Fu, P., Jiang, Q., Yang, T., Li, J., and Ge, X.: The impact of relative
715 humidity on aerosol composition and evolution processes during wintertime in Beijing,
716 China, Atmos. Environ., 77, 927-934, 10.1016/j.atmosenv.2013.06.019, 2013.

717 Stein, U., and Alpert, P.: Factor separation in numerical simulations, Journal of the
718 Atmospheric Science, 50, 2107-2115, 10.1175/1520-0469(1993)
719 050<2107:fsins>2.0.co;2, 1993.

720 Tao, J. C., Zhao, C. S., Ma, N., and Liu, P. F.: The impact of aerosol hygroscopic growth on
721 the single-scattering albedo and its application on the NO_2 photolysis rate coefficient,
722 Atmos. Chem. Phys., 14, 12055-12067, 10.5194/acp-14-12055-2014, 2014.

723 Tie, X. X., Huang, R. J., Cao, J. J., Zhang, Q., Cheng, Y. F., Su, H., Chang, D., Poschl, U.,
724 Hoffmann, T., Dusek, U., Li, G. H., Worsnop, D. R., and O'Dowd, C. D.: Severe
725 Pollution in China Amplified by Atmospheric Moisture, Sci. Rep., 7, 8,
726 10.1038/s41598-017-15909-1, 2017.

727 Volkamer, R., Martini, F. S., Molina, L. T., Salcedo, D., Jimenez, J. L., and Molina, M. J.: A
728 missing sink for gas-phase glyoxal in Mexico City: Formation of secondary organic
729 aerosol, Geophys. Res. Lett., 34, 5, 10.1029/2007gl030752, 2007.

730 Wang, G., Zhang, R., Gomez, M. E., Yang, L., Zamora, M. L., Hu, M., Lin, Y., Peng, J., Guo,
731 S., and Meng, J.: Persistent sulfate formation from London Fog to Chinese haze, P. Natl.
732 Acad. Sci. USA., 113, 13630–13635, 2016.

733 Wang, Y. S., Yao, L., Wang, L. L., Liu, Z. R., Ji, D. S., Tang, G. Q., Zhang, J. K., Sun, Y.,
734 Hu, B., and Xin, J. Y.: Mechanism for the formation of the January 2013 heavy haze
735 pollution episode over central and eastern China, Sci. China-Earth Sci., 57, 14-25,
736 10.1007/s11430-013-4773-4, 2014.

737 Weinhold, B.: Ozone nation – EPA standard panned by the people, Environ. Health. Persp.,
738 116, A302–A305, 2008.

739 Wu, J. R., Li, G. H., Cao, J. J., Bei, N. F., Wang, Y. C., Feng, T., Huang, R. J., Liu, S. X.,
740 Zhang, Q., and Tie, X. X.: Contributions of trans-boundary transport to summertime air
741 quality in Beijing, China, Atmos. Chem. Phys., 17, 2035-2051,
742 10.5194/acp-17-2035-2017, 2017.

743 Wu, P., Ding, Y. H., and Liu, Y. J.: Atmospheric circulation and dynamic mechanism for
744 persistent haze events in the Beijing-Tianjin-Hebei region, Adv. Atmos. Sci., 34,
745 429-440, 10.1007/s00376-016-6158-z, 2017.

746 Wu, Z. J., Wang, Y., Tan, T. Y., Zhu, Y. S., Li, M. R., Shang, D. J., Wang, H. C., Lu, K. D.,
747 Guo, S., Zeng, L. M., and Zhang, Y. H.: Aerosol Liquid Water Driven by
748 Anthropogenic Inorganic Salts: Implying Its Key Role in Haze Formation over the
749 North China Plain, Environ. Sci. Technol. Lett., 5, 160-166, 10.1021/acs.estlett.8b00021,
750 2018.

751 Xing, L., Wu, J., Elser, M., Tong, S., Liu, S., Li, X., Liu, L., Cao, J., Zhou, J., El-Haddad, I.,
752 Huang, R., Ge, M., Tie, X., Prévôt, A. S. H., and Li, G.: Wintertime secondary organic
753 aerosol formation in Beijing-Tianjin-Hebei (BTH): Contributions of HONO sources and
754 heterogeneous reactions, Atmos. Chem. Phys. Discuss., 2018, 1-25,

10.5194/acp-2018-770, 2018.

Xu, J. W., Martin, R. V., van Donkelaar, A., Kim, J., Choi, M., Zhang, Q., Geng, G., Liu, Y., Ma, Z., Huang, L., Wang, Y., Chen, H., Che, H., Lin, P., and Lin, N.: Estimating ground-level PM2.5 in eastern China using aerosol optical depth determined from the GOCI satellite instrument, Atmos. Chem. Phys., 15, 13133-13144, 10.5194/acp-15-13133-2015, 2015.

Zhang, L., Sun, J. Y., Shen, X. J., Zhang, Y. M., Che, H., Ma, Q. L., Zhang, Y. W., Zhang, X. Y., and Ogren, J. A.: Observations of relative humidity effects on aerosol light scattering in the Yangtze River Delta of China, Atmos. Chem. Phys., 15, 8439-8454, 10.5194/acp-15-8439-2015, 2015.

Zhang, Q., Streets, D. G., Carmichael, G. R., He, K. B., Huo, H., Kannari, A., Klimont, Z., Park, I. S., Reddy, S., Fu, J. S., Chen, D., Duan, L., Lei, Y., Wang, L. T., and Yao, Z. L.: Asian emissions in 2006 for the NASA INTEX-B mission, Atmos. Chem. Phys., 9, 5131-5153, https://doi.org/10.5194/acp-9-5131-2009, 2009.

Zhang, R. H., Li, Q., and Zhang, R. N.: Meteorological conditions for the persistent severe fog and haze event over eastern China in January 2013, Sci. China-Earth Sci., 57, 26-35, 10.1007/s11430-013-4774-3, 2014.

Zhang, R., Jing, J., Tao, J., Hsu, S.-C., Wang, G., Cao, J., Lee, C. S. L., Zhu, L., Chen, Z., Zhao, Y., and Shen, Z.: Chemical characterization and source apportionment of $PM_{2.5}$ in Beijing: seasonal perspective, Atmos. Chem. Phys., 13, 7053–7074, https://doi.org/10.5194/acp-13-7053-2013, 2013.

Zhao, J., Levitt, N. P., Zhang, R. Y., and Chen, J. M.: Heterogeneous reactions of methylglyoxal in acidic media: implications for secondary organic aerosol formation, Environ. Sci. Technol., 40, 7682–7687, 2006.

Zhou, Y., Zhang, H. F., Parikh, H. M., Chen, E. H., Rattanavaraha, W., Rosen, E. P., Wang, W. X., and Kamens, R. M.: Secondary organic aerosol formation from xylenes and mixtures of toluene and xylenes in an atmospheric urban hydrocarbon mixture: Water and particle seed effects (II), Atmos. Environ., 45, 3882-3890, 10.1016/j.atmosenv.2010.12.048, 2011.

785 Table 1 WRF-Chem model configurations
786

Regions	East Asia
Simulation period	December 05, 2015 - January 04, 2016
Domain size	400 × 400
Domain center	35°N, 114°E
Horizontal resolution	12km × 12km
Vertical resolution	35 vertical levels with a stretched vertical grid with spacing ranging from 30 m near the surface, to 500 m at 2.5 km and 1 km above 14 km
Microphysics scheme	WSM 6-class graupel scheme (Hong and Lim, 2006)
Boundary layer scheme	MYJ TKE scheme (Janjić, 2002)
Surface layer scheme	MYJ surface scheme (Janjić, 2002)
Land-surface scheme	Unified Noah land-surface model (Chen and Dudhia, 2001)
Longwave radiation scheme	Goddard longwave scheme (Chou and Suarez, 2001)
Shortwave radiation scheme	Goddard shortwave scheme (Chou and Suarez, 1999)
Meteorological boundary and initial conditions	NCEP 1°×1° reanalysis data
Chemical initial and boundary conditions	MOZART 6-hour output (Horowitz et al., 2003)
Anthropogenic emission inventory	Developed by Zhang et al. (2009) and Li et al. (2017), 2012 base year, and SAPRC-99 chemical mechanism
Biogenic emission inventory	MEGAN model developed by Guenther et al. (2006)
Model spin-up time	28 hours

787
788
789
790
791

Table 2 Description of the sensitivity simulations.

Case	Aerosol hygroscopic growth	ALW contribution to AOD		Multiphase reactions involving the ALW
		in the ARF	in the photolysis	
f_{base}	On	On	On	On
f_{alw_rad0}	On	Off	On	On
f_{alw_j0}	On	On	Off	On
f_{alw_het0}	On	On	On	Off
f_{alw_tot0}	On	Off	Off	Off

Figure Captions

Figure 1 (a) WRF-Chem simulation domain with topography and (b) North China Plain. In (a), the blue circles represent centers of cities with ambient monitoring sites and the size of circles denotes the number of ambient monitoring sites of cities. In (b), the red capitals denote six typical polluted cities in NCP. A: Beijing; B: Tianjin; C: Shijiazhuang; D: Baoding; E: Tangshan; F: Chengde. The blue numbers denote the CERN sites with the hourly RH measurement. 1: Jiaozhouwan; 2: Yucheng; 3: Luancheng.

Figure 2 Scatter plots of near-surface [$PM_{2.5}$] and RH at six typical polluted cities in NCP during the 2015 wintertime. The red diamond shows the bin average of near-surface [$PM_{2.5}$], and the red line denotes the variation of the bin average of near-surface [$PM_{2.5}$] with RH.

Figure 3 Comparison of measured (black dots) and predicted (red line) diurnal profiles of the RH in (a) Luancheng, (b) Yucheng, and (c) Jiaozhouwan from 05 December 2015 to 04 January 2016.

Figure 4 Spatial distribution of (a) NCEP reanalyzed and (b) simulated RH averaged from 05 December 2015 to 04 January 2016.

Figure 5 Average (a) absolute and (b) relative AOD contribution caused by the ALW from 05 December 2015 to 04 January 2016.

Figure 6 Average near-surface (a) absolute and (b) relative $PM_{2.5}$ contribution caused by the ALW-ARF from 05 December 2015 to 04 January 2016.

Figure 7 Average variations of (a) AOD and (b) Reff in $\mathbf{f_{base}}$ (red line) and $\mathbf{f_{alw\_rad0}}$ (blue line) as a function of bin [$PM_{2.5}$] in NCP during daytime from 05 December 2015 to 04 January 2016.

Figure 8 Average (a) percentage decrease of SWDOWN at the ground surface, (b) decrease of TSFC, (c) percentage decrease of PBLH, and (d) percentage contribution of near-surface [$PM_{2.5}$] caused by the ALW-ARF, as a function of the near-surface [$PM_{2.5}$] in NCP during daytime from 05 December 2015 to 04 January 2016.

Figure 9 Average variations of daytime (a)/(b) NO_2 photolysis and (c)/(d) O_3 concentration at $1^{st}/5^{th}$ model layer (around 18 m and 420 m above the ground surface, respectively) caused by the ALW from 05 December 2015 to 04 January 2016 in NCP.

Figure 10 Average near-surface (a) absolute and (b) relative $PM_{2.5}$ contribution caused by the ALW-J from 05 December 2015 to 04 January 2016.

Figure 11 Average near-surface (a)/(c)/(e) absolute and (b)/(d)/(f) relative contribution to sulfate/nitrate/ammonium concentrations, caused by the ALW-HET from 05 December 2015 to 04 January 2016.

Figure 12 Spatial distribution of NH_3 emission rate in December.

Figure 13 Average near-surface (a) absolute and (b) relative SOA contribution caused by the ALW-HET from 05 December 2015 to 04 January 2016.

Figure 14 Average near-surface (a) absolute and (b) relative $PM_{2.5}$ contribution caused by the ALW-HET from 05 December 2015 to 04 January 2016.

Figure 15 Average percentage decrease of (a) BC and (b) POA concentrations caused by the ALW-HET, as a function of the near-surface [$PM_{2.5}$] in NCP from 05 December 2015 to 04 January 2016.

Figure 16 Average variations of (a) AOD and (b) Reff in f_{base} (red line) and f_{alw_het0} (blue line), respectively, and average percentage decrease of near-surface (c) aerosol number concentration and (d) surface area caused by the ALW-HET, as a function of bin [$PM_{2.5}$] in NCP from 05 December 2015 to 04 January 2016.

Figure 17 Average (a) percentage decrease of SWDOWN at the ground surface, (b) decrease of TSFC, and (c) percentage decrease of PBLH caused by the ALW-HET, as a function of the near-surface [$PM_{2.5}$] in NCP during daytime from 05 December 2015 to 04 January 2016.

Figure 18 Average near-surface (a) absolute and (b) relative $PM_{2.5}$ contribution caused by the ALW-TOT from 05 December 2015 to 04 January 2016.

Figure 19 Average contributions to near-surface [$PM_{2.5}$] caused by the ALW-TOT (black line), ALW-HET (red line), ALW-RAD (green line), and ALW-J (blue line), respectively, as a function of the RH in NCP from 05 December 2015 to 04 January 2016.

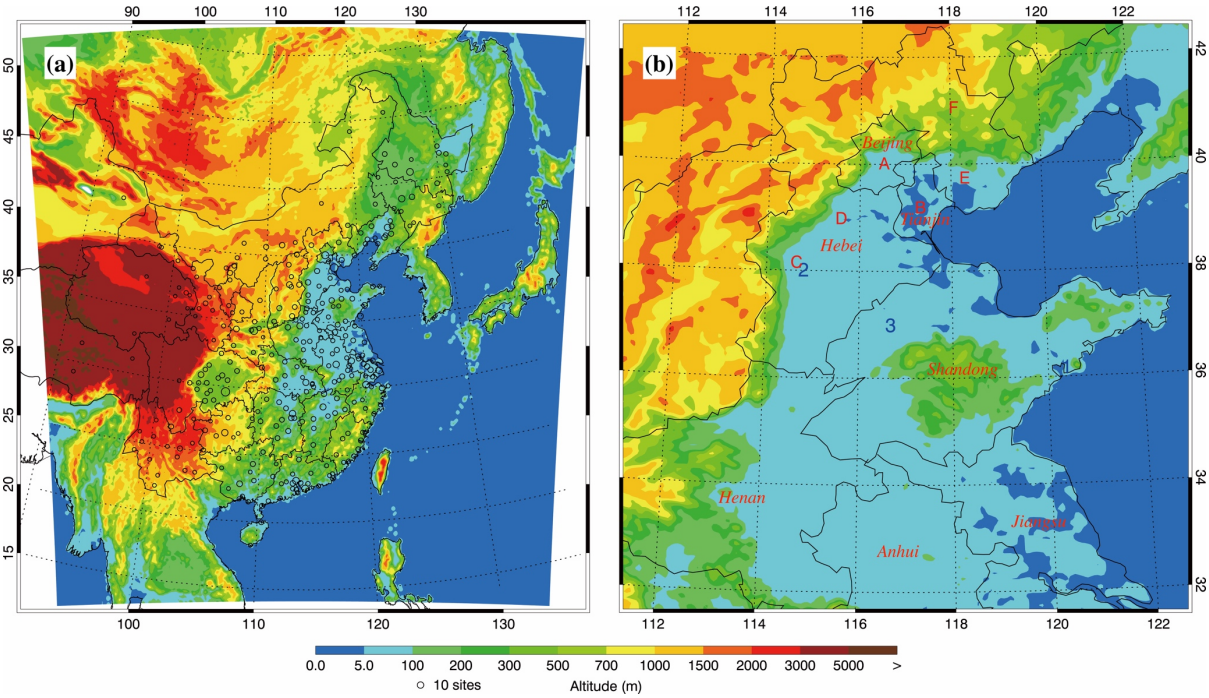

Figure 1 (a) WRF-Chem simulation domain with topography and (b) North China Plain. In (a), the blue circles represent centers of cities with ambient monitoring sites and the size of blue circles denotes the number of ambient monitoring sites of cities. In (b), the red capitals denote six typical polluted cities in NCP. A: Beijing; B: Tianjin; C: Shijiazhuang; D: Baoding; E: Tangshan; F: Chengde. The blue numbers denote the CERN sites with the RH measurement. 1: Jiaozhouwan; 2: Yucheng; 3: Luancheng.

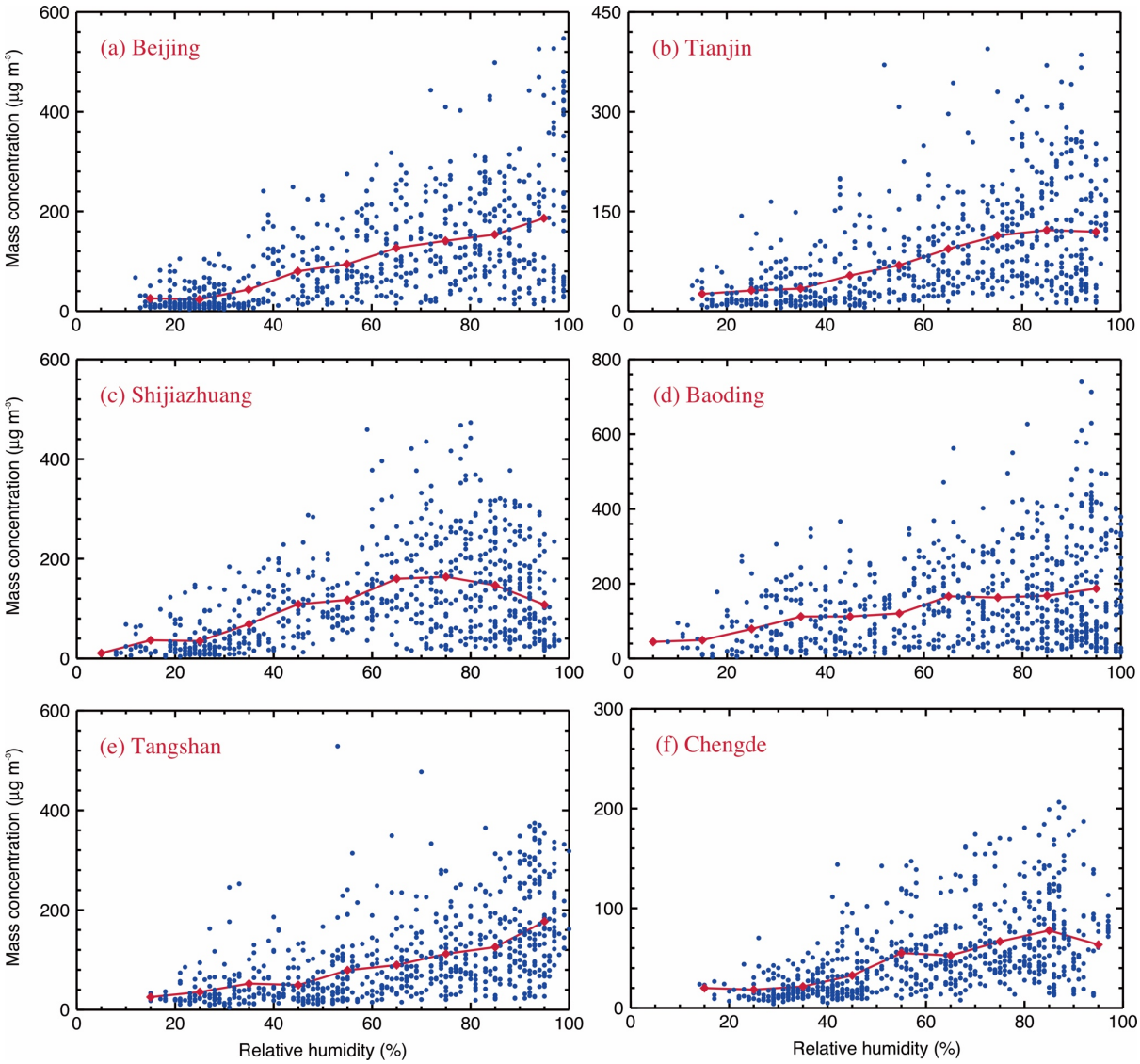

Figure 2 Scatter plots of near-surface [$PM_{2.5}$] and RH at six typical polluted cities in NCP during the 2015 wintertime. The red diamond shows the bin average of near-surface [$PM_{2.5}$], and the red line denotes the variation of the bin average of near-surface [$PM_{2.5}$] with RH.

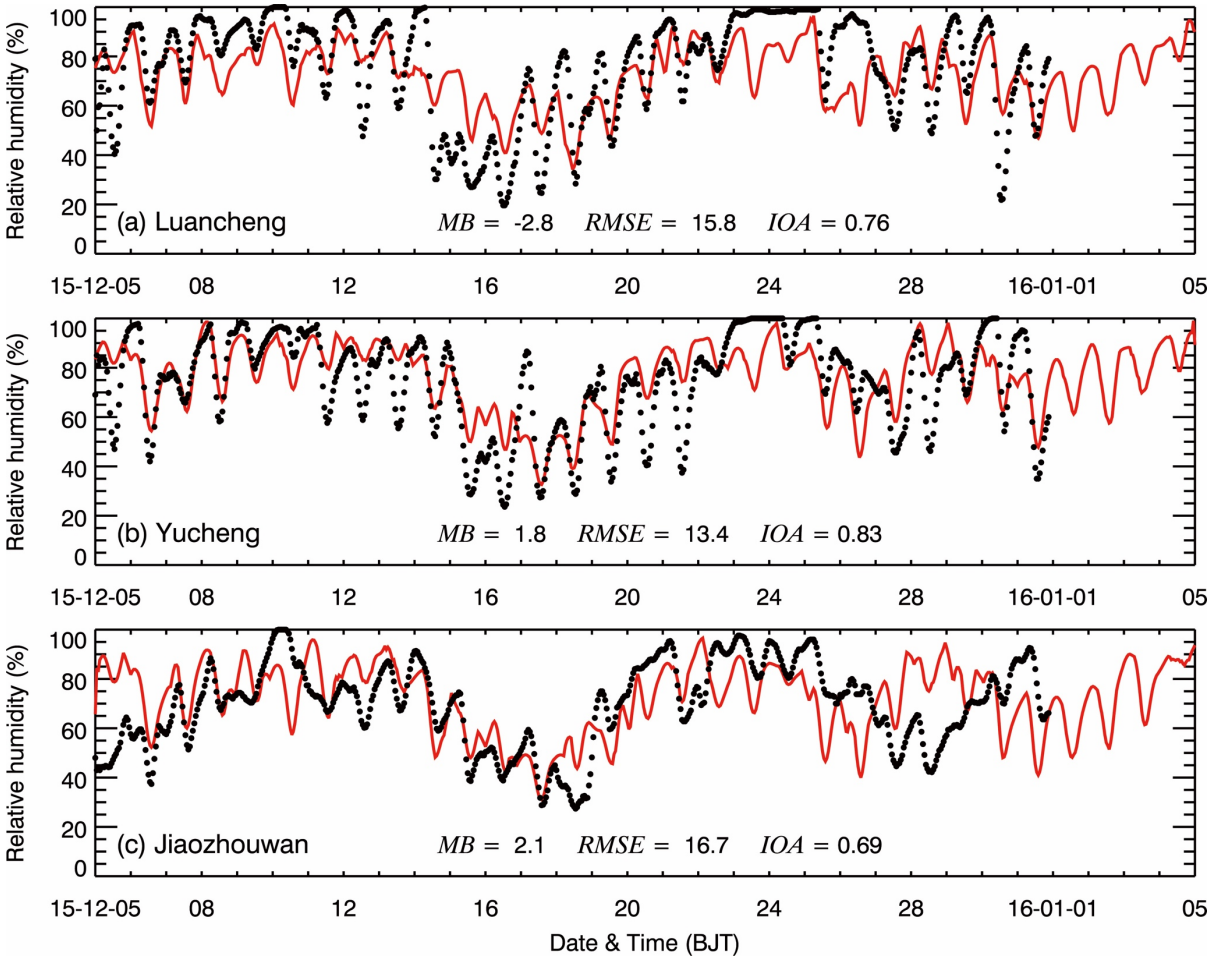

Figure 3 Comparison of measured (black dots) and predicted (red line) diurnal profiles of the RH in (a) Luancheng, (b) Yucheng, and (c) Jiaozhouwan from 05 December 2015 to 04 January 2016.

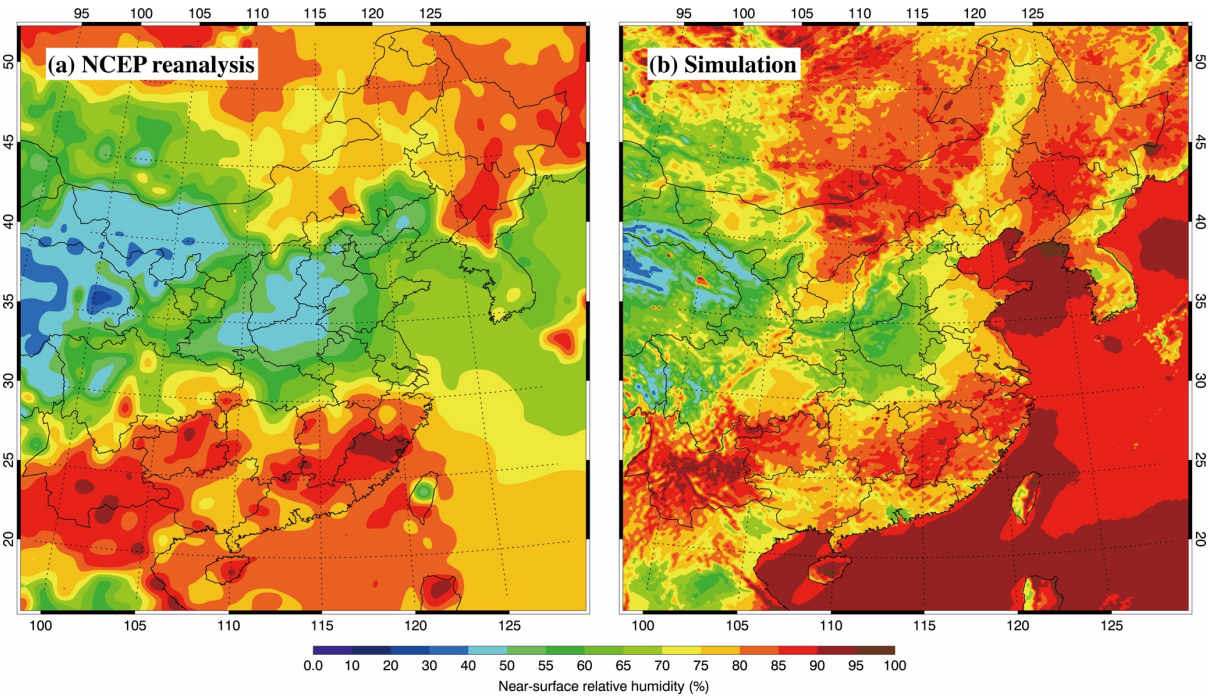

Figure 4 Spatial distribution of (a) NCEP reanalyzed and (b) simulated RH averaged from 05 December 2015 to 04 January 2016.

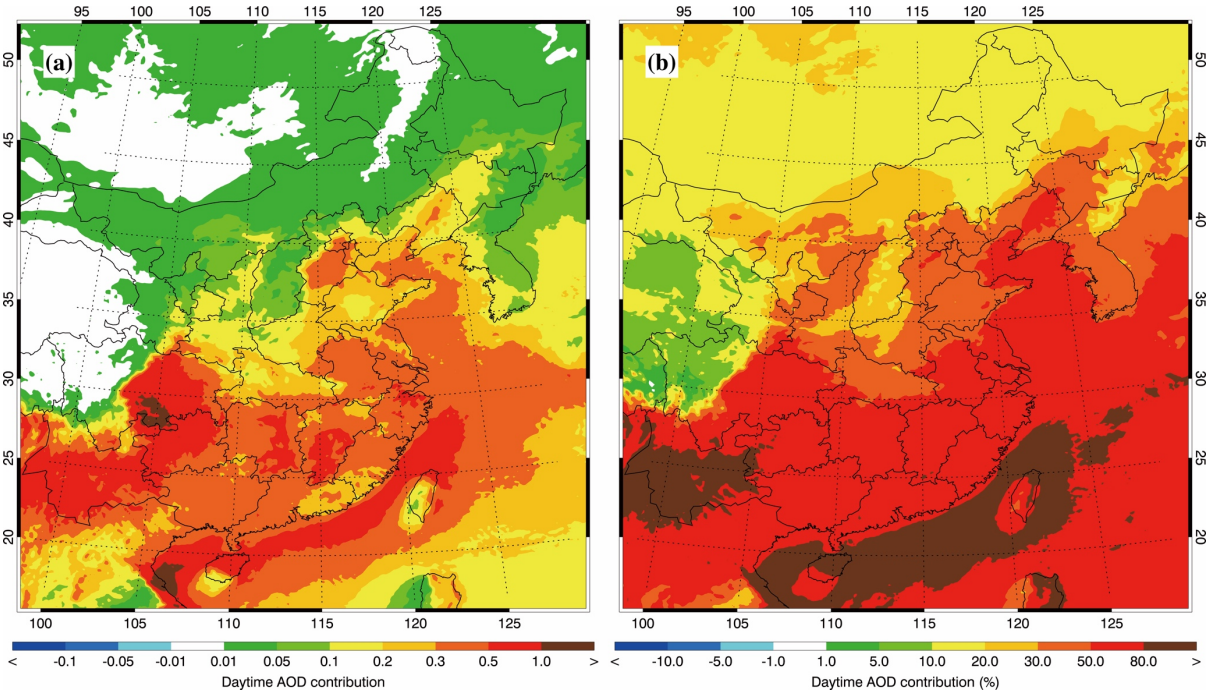

Figure 5 Average (a) absolute and (b) relative AOD contribution caused by the ALW from 05 December 2015 to 04 January 2016.

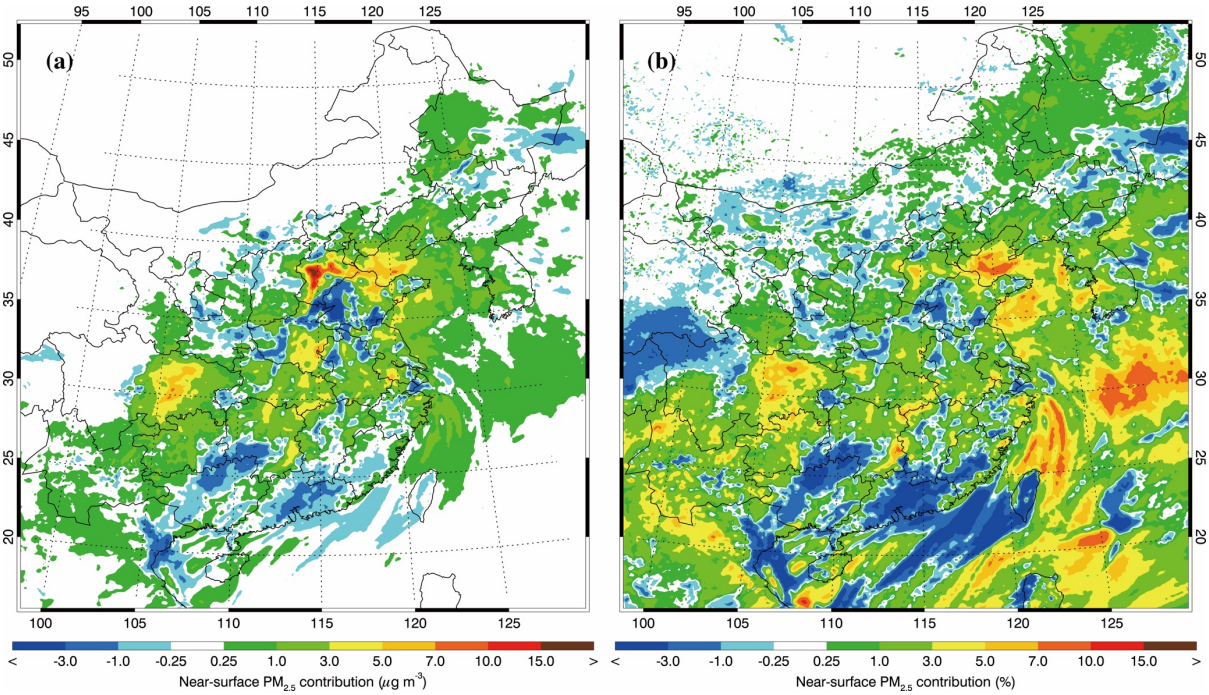

Figure 6 Average near-surface (a) absolute and (b) relative $PM_{2.5}$ contribution caused by the ALW-ARF from 05 December 2015 to 04 January 2016.

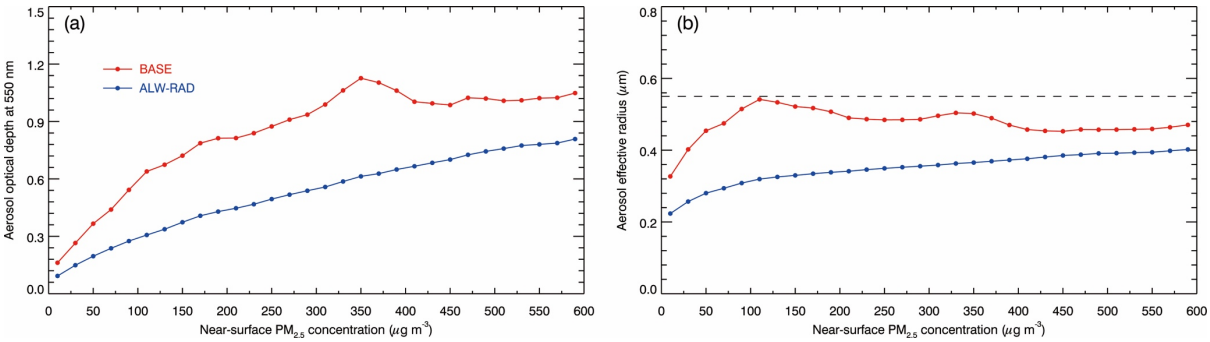

Figure 7 Average variations of (a) AOD and (b) Reff in $\mathbf{f_{base}}$ (red line) and $\mathbf{f_{alw\_rad0}}$ (blue line) as a function of bin [$PM_{2.5}$] in NCP during daytime from 05 December 2015 to 04 January 2016.

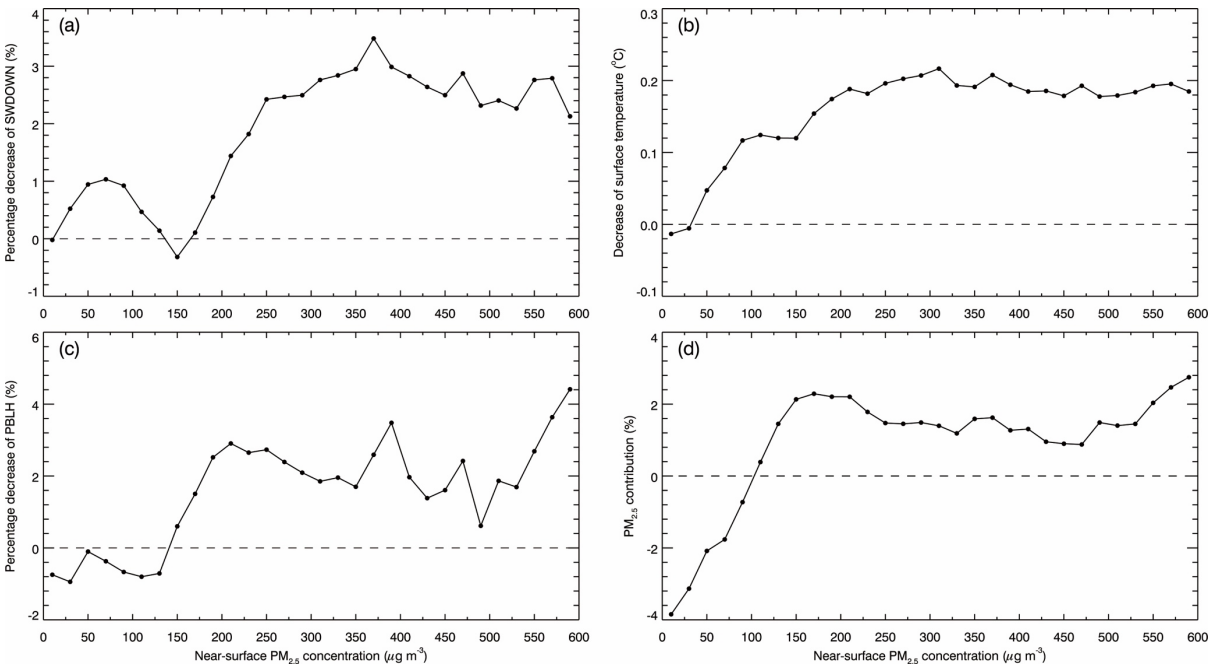

Figure 8 Average (a) percentage decrease of SWDOWN at the ground surface, (b) decrease of TSFC, (c) percentage decrease of PBLH, and (d) percentage contribution of near-surface [$PM_{2.5}$] caused by the ALW-ARF, as a function of the near-surface [$PM_{2.5}$] in NCP during daytime from 05 December 2015 to 04 January 2016.

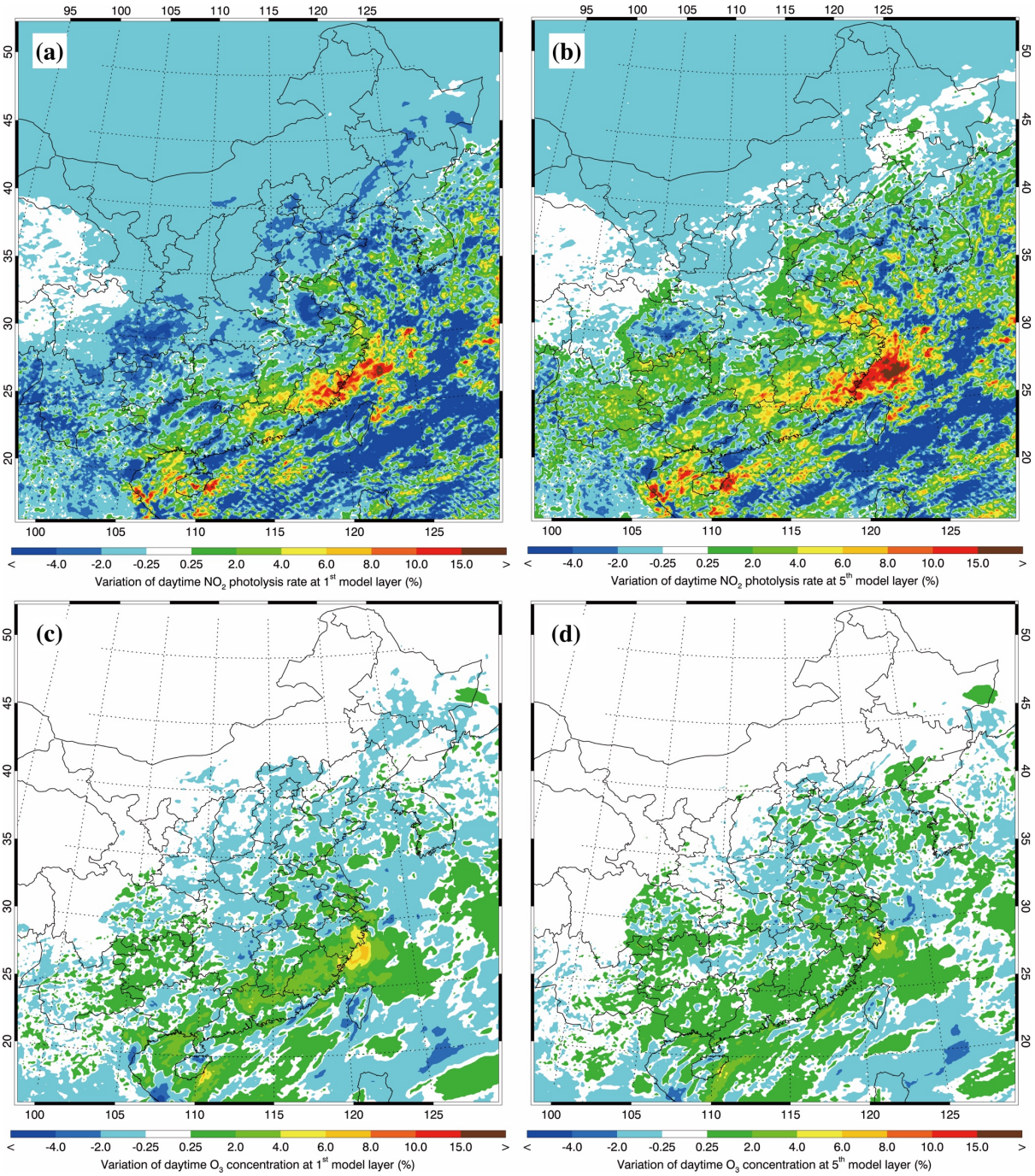

Figure 9 Average variations of daytime (a)/(b) NO_2 photolysis and (c)/(d) O_3 concentration at $1^{st}/5^{th}$ model layer (around 18 m and 420 m above the ground surface, respectively) caused by the ALW from 05 December 2015 to 04 January 2016 in NCP.

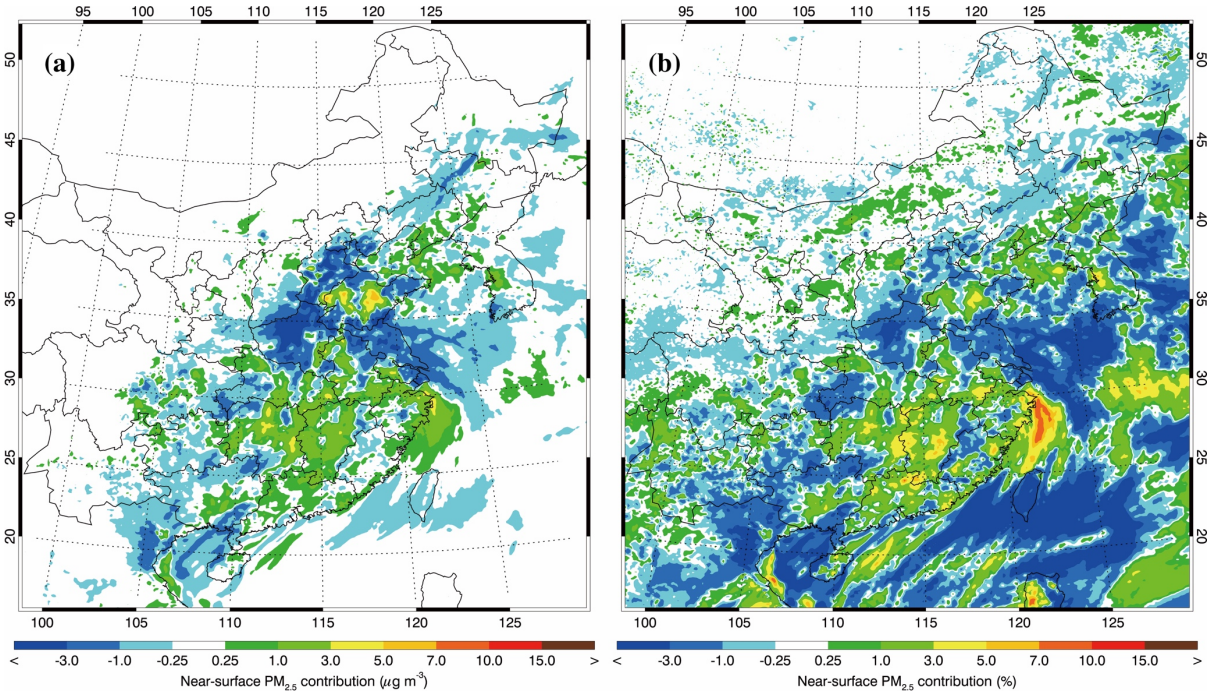

Figure 10 Average near-surface (a) absolute and (b) relative $PM_{2.5}$ contribution caused by the ALW-J from 05 December 2015 to 04 January 2016.

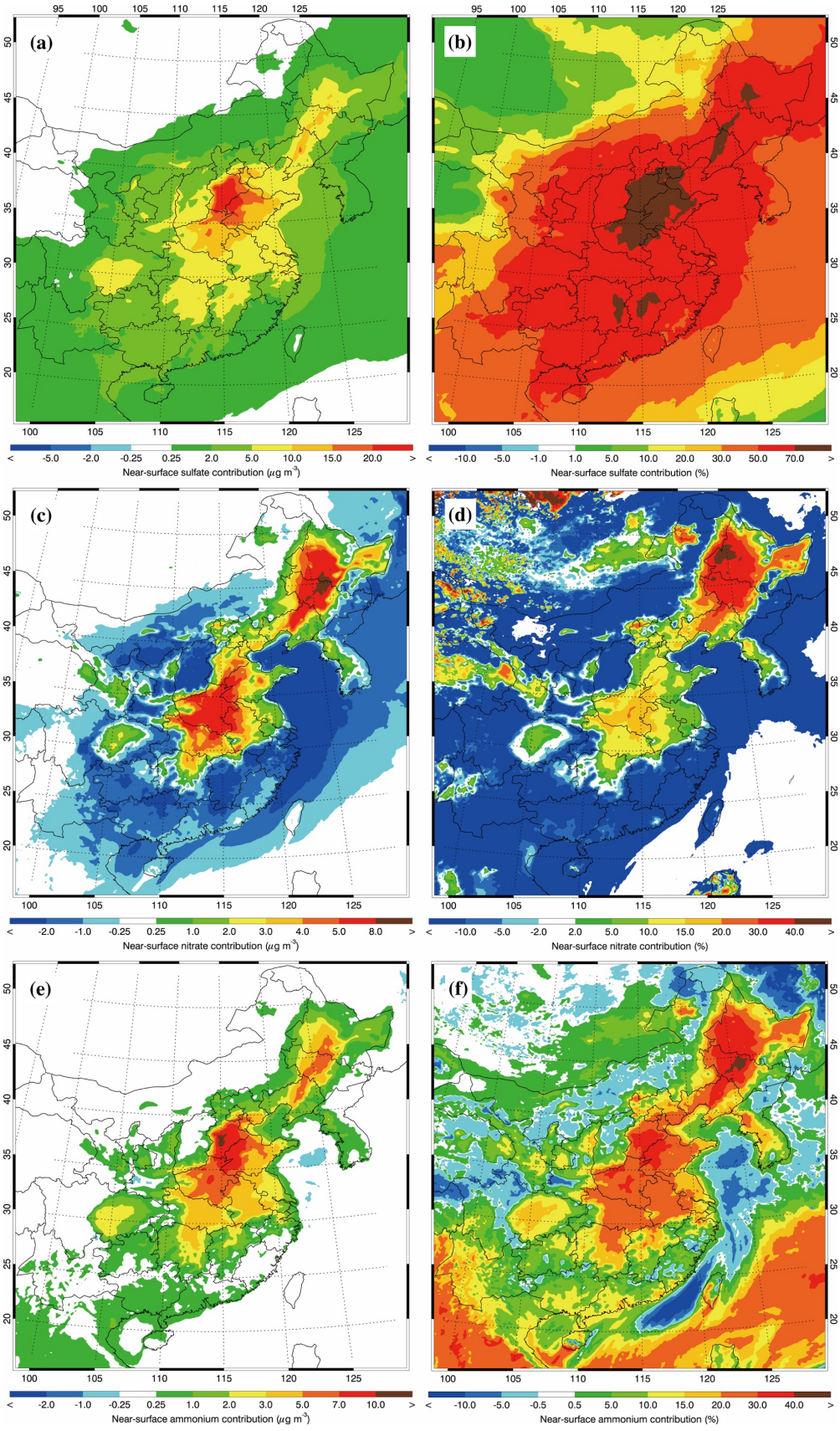

Figure 11 Average near-surface (a)/(c)/(e) absolute and (b)/(d)/(f) relative contribution to sulfate/nitrate/ammonium concentrations, caused by the ALW-HET from 05 December 2015 to 04 January 2016.

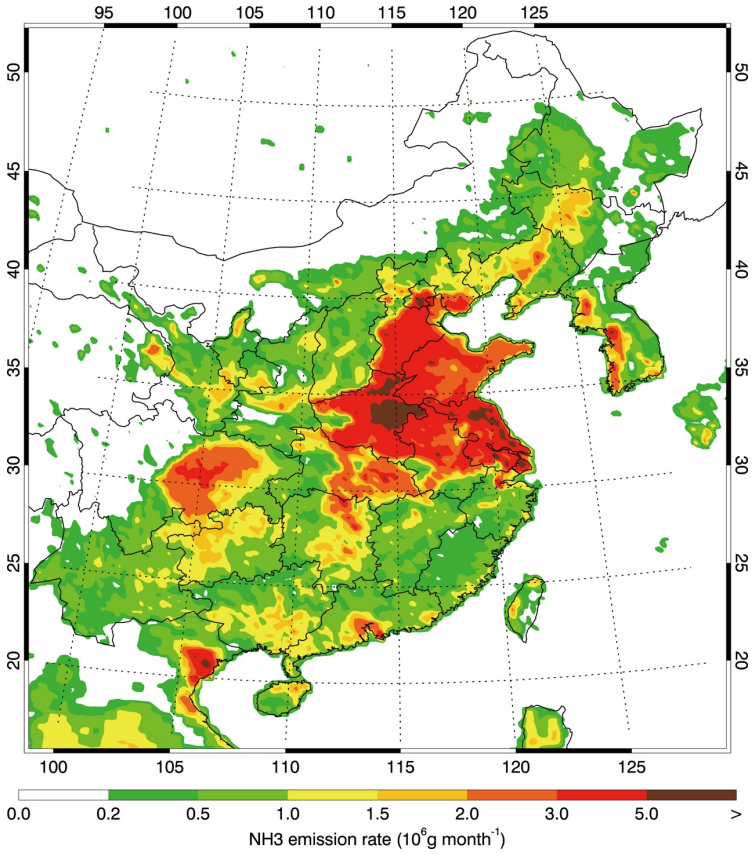

Figure 12 Spatial distribution of NH_3 emission rate in December.

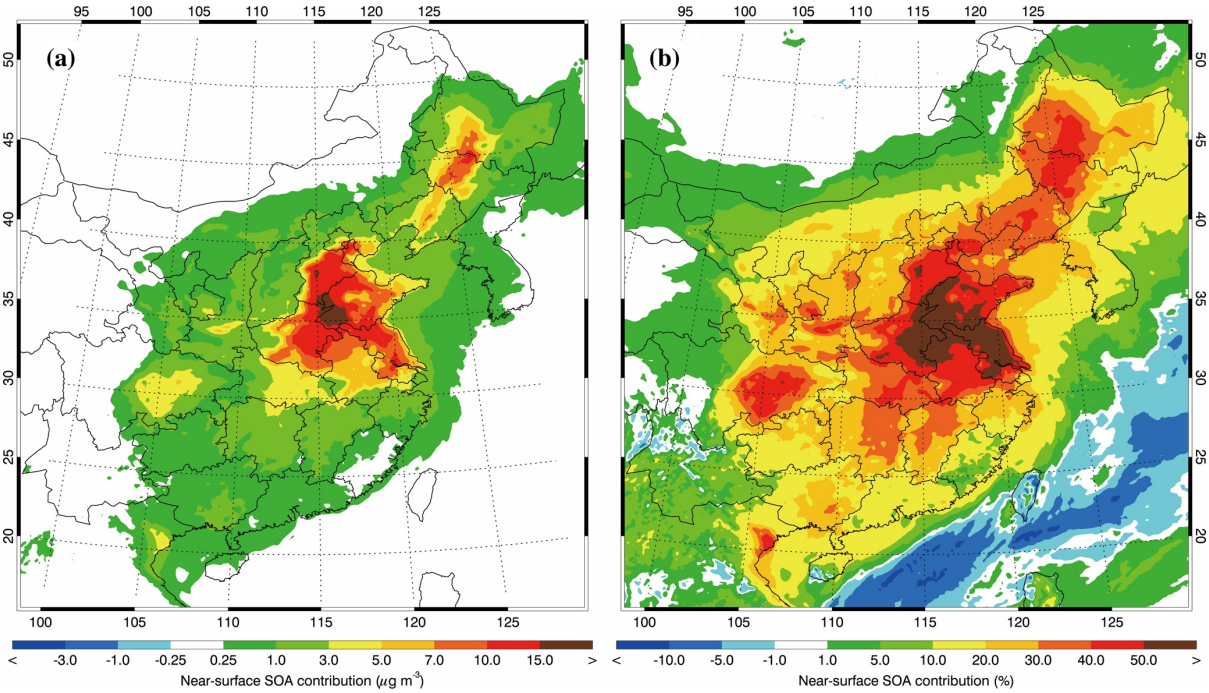

Figure 13 Average near-surface (a) absolute and (b) relative SOA contribution caused by the ALW-HET from 05 December 2015 to 04 January 2016.

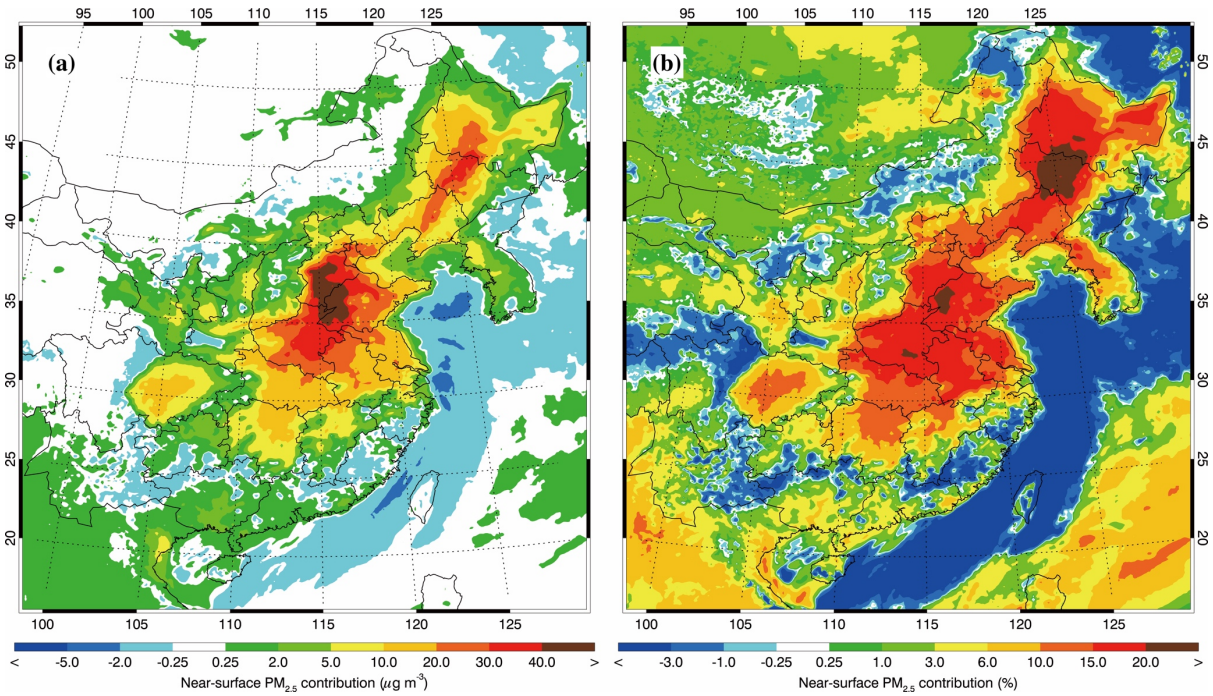

Figure 14 Average near-surface (a) absolute and (b) relative $PM_{2.5}$ contribution caused by the ALW-HET from 05 December 2015 to 04 January 2016.

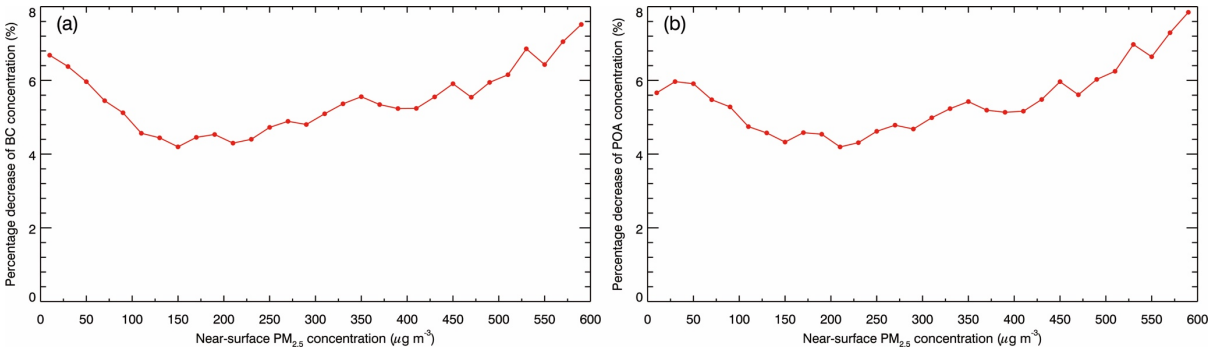

Figure 15 Average percentage decrease of (a) BC and (b) POA concentrations caused by the ALW-HET, as a function of the near-surface [$PM_{2.5}$] in NCP from 05 December 2015 to 04 January 2016.

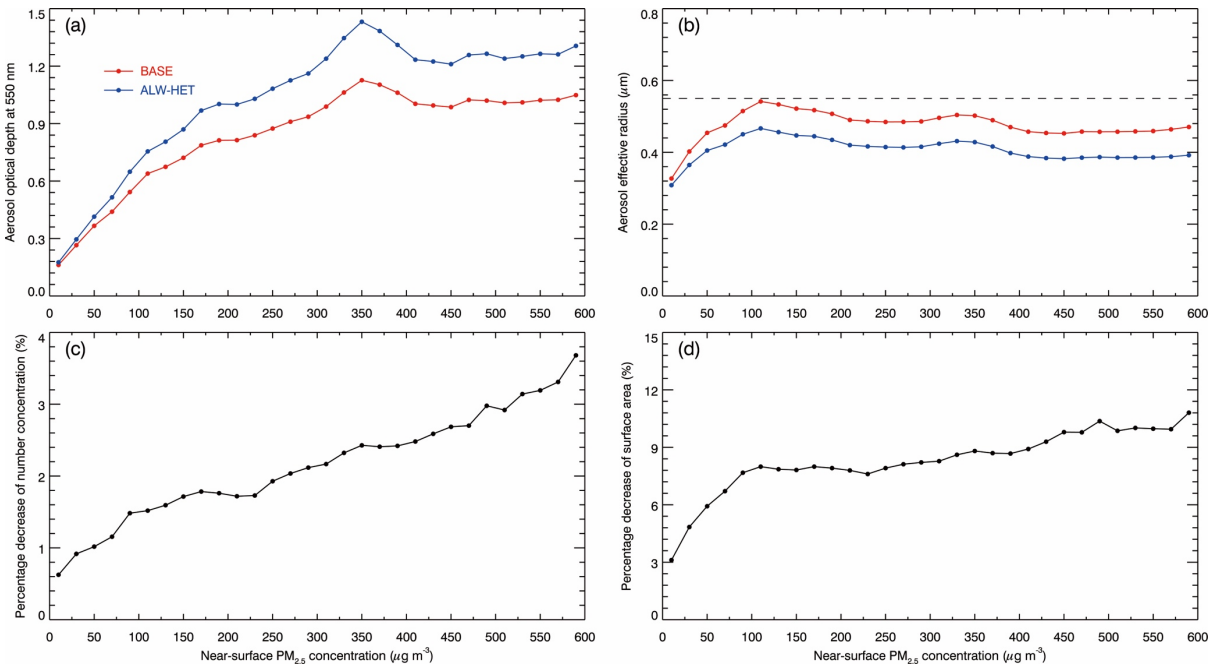

Figure 16 Average variations of (a) AOD and (b) Reff in f_{base} (red line) and f_{alw_het0} (blue line), respectively, and average percentage decrease of near-surface (c) aerosol number concentration and (d) surface area caused by the ALW-HET, as a function of bin [$PM_{2.5}$] in NCP from 05 December 2015 to 04 January 2016.

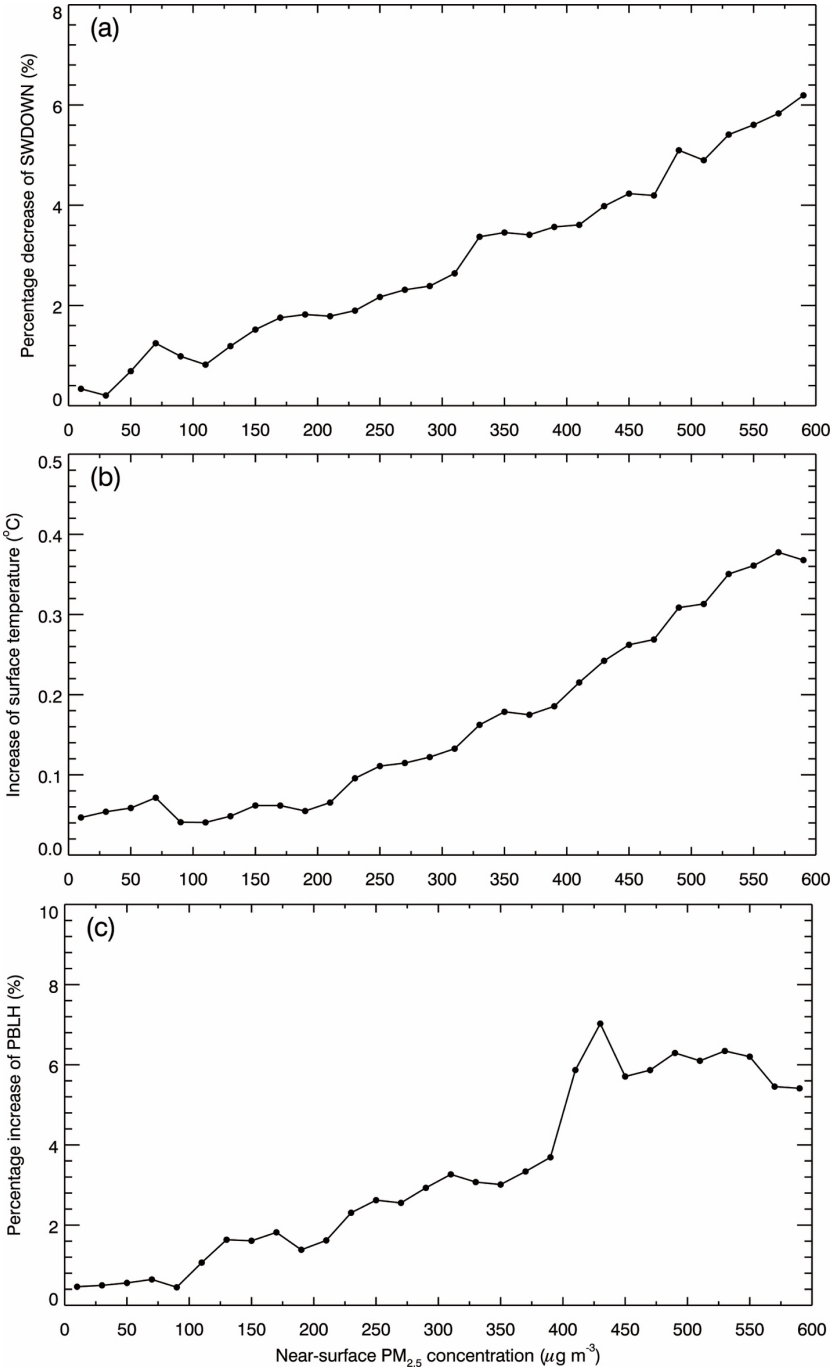

Figure 17 Average (a) percentage decrease of SWDOWN at the ground surface, (b) decrease of TSFC, and (c) percentage decrease of PBLH caused by the ALW-HET, as a function of the near-surface [$PM_{2.5}$] in NCP during daytime from 05 December 2015 to 04 January 2016.

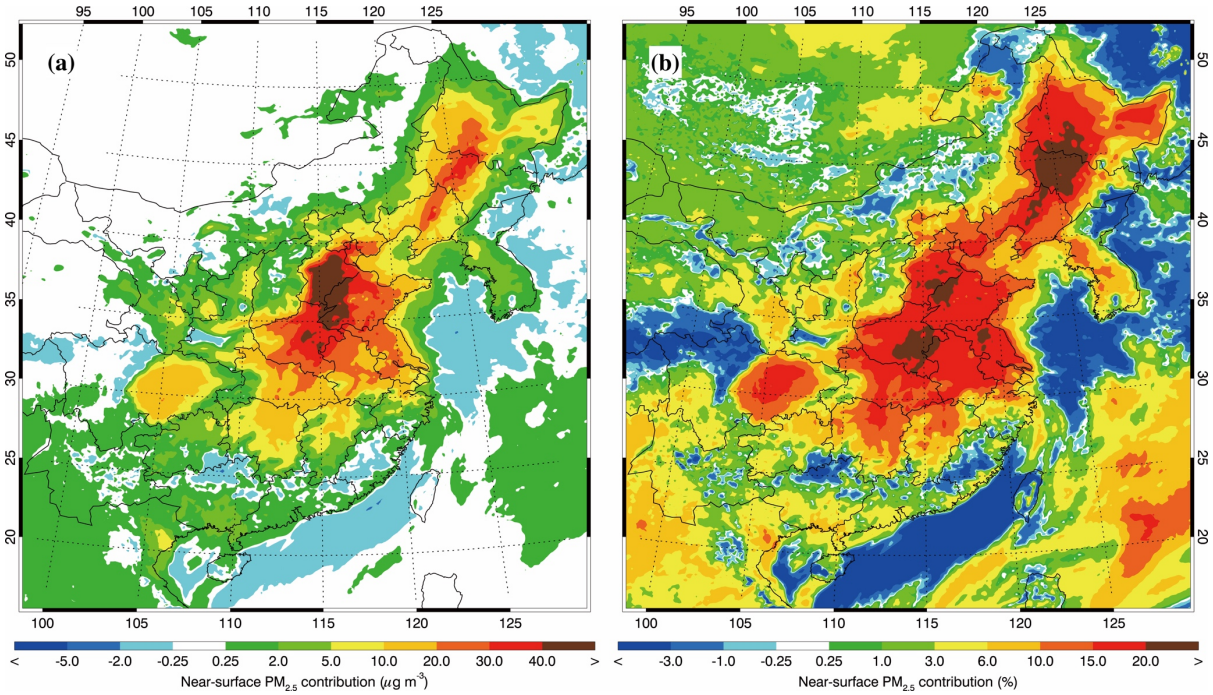

Figure 18 Average near-surface (a) absolute and (b) relative $PM_{2.5}$ contribution caused by the ALW-TOT from 05 December 2015 to 04 January 2016.

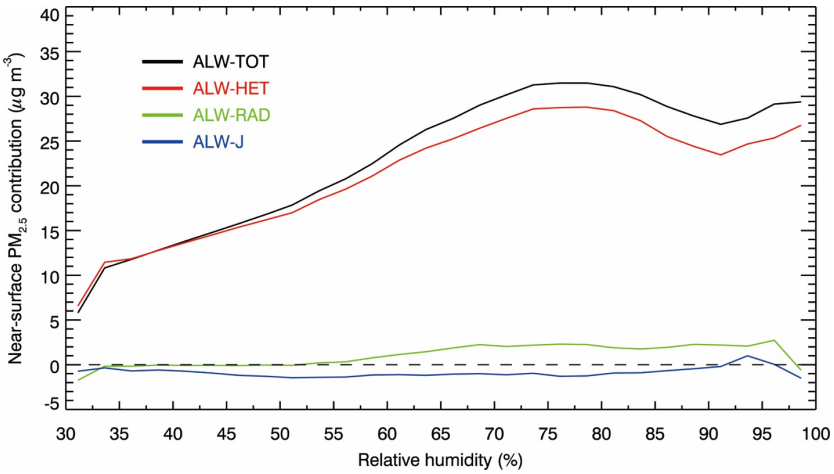

Figure 19 Average contributions to the near-surface [$PM_{2.5}$] caused by the ALW-TOT (black line), ALW-HET (red line), ALW-RAD (green line), and ALW-J (blue line), respectively, as a function of the RH in NCP from 05 December 2015 to 04 January 2016.